

Fast and spectrally accurate summation of 2-periodic Stokes potentials

Dag Lindbo^{1,*} and Anna-Karin Tornberg¹

¹*Numerical Analysis, Royal Inst. of Tech. (KTH), 100 44 Stockholm, Sweden*

November 3, 2018

Abstract

We derive a Ewald decomposition for the Stokeslet in planar periodicity and a novel PME-type $\mathcal{O}(N \log N)$ method for the fast evaluation of the resulting sums. The decomposition is the natural 2P counterpart to the classical 3P decomposition by Hasimoto, and is given in an explicit form not found in the literature. Truncation error estimates are provided to aid in selecting parameters. The fast, PME-type, method appears to be the first fast method for computing Stokeslet Ewald sums in planar periodicity, and has three attractive properties: it is spectrally accurate; it uses the minimal amount of memory that a gridded Ewald method can use; and provides clarity regarding numerical errors and how to choose parameters. Analytical and numerical results are given to support this. We explore the practicalities of the proposed method, and survey the computational issues involved in applying it to 2-periodic boundary integral Stokes problems.

1 Introduction

Viscous flow systems continuously enjoy much attention from various scientific disciplines, such as the widespread study of passive and motile suspensions and other applications in bio-, micro- and complex fluidics. An example is the large body of work that involves the study of locomotion of small organisms, the basics of which are illustrated in a classic article by Purcell [55], with further developments in e.g. Koiller et al. [37]. Theoretical understanding of various modes of propulsion [66, 65, 17, 8, 30, 29] is rapidly progressing apace with simulation methods [32, 59]. If history is any guide, analytical results will feed into computational models and rich computational studies of complex systems will emerge. There are also notably strong interdisciplinary connections present in this area. A recent survey of the modelling of biomimetic fluid flow by Saha et al. [57] provides a broader perspective, including modeling and computation outside of the viscous flow regime.

Another area where there has been much activity is in simulation of suspensions of various particles in viscous flows, motivated, for instance, by a desire to understand the formation of microstructures [27] and paper-making [46]. Here one finds detailed computational studies of rigid or flexible fiber suspension, such as the work by Saintillan et al. [58] and Tornberg,

*To whom correspondence should be addressed. Email: dag@kth.se

Shelley and collaborators [69, 68, 61], as well as large body of work concerning suspensions of various spheroids [7, 64] and related particles [41]. Complex structure formation is observed, based on accurate modeling of hydrodynamical interactions, in these computational investigations.

Alas, the present work shall not in itself elucidate these fascinating questions of collective dynamics, but rather pursue algorithmic development that could help such investigations deal with larger systems in future.

The models under consideration in the works cited, and in countless other investigations, are based on the Stokes equations. A variety of numerical and analytical techniques are used, but a common feature is the use of singularity solutions. One class of methods is the so called distributed singularity approach, in which the various Green’s functions of Stokes equations are combined in point, line, or surface distributions to generate the flow induced by a particular particle or distribution. In this way, slender bodies (e.g. fibers) are represented by a line distribution of Stokes potentials along its centerline, as was suggested by Batchelor [3]. In an analogous way, spheroids can be represented by a combination of higher-order Green’s functions, see e.g. Zhou & Pozrikidis [73] and Götz [18].

There are also direct boundary integral methods, as discussed in e.g. Pozrikidis [53, 51], Anderson et al. [31, 5, 4], and others [35, 71, 72]. Another class of methods that has been highly successful is known as *Stokesian dynamics*, and is due to Brady and collaborators [6, 64]. All of these methods are based on distributions of Green’s functions that are either summed or integrated, often in intricate ways.

Moreover, results free from finite-size effects are often of interest; the well-trodden path towards which is applying periodic boundary conditions to a sufficiently large system [64, 69, 58]. Solvers that exploit periodic structure, such as the fast Ewald methods that we shall survey shortly, are often highly specialized. In particular, there are fundamental differences between how full (i.e. applied in all three directions) and lower dimensional periodicity (i.e. periodicity with respect to one or two dimensions) enters in mathematical (cf. Pozrikidis [52]) and algorithmic terms. Whereas methods are relatively well established for fully periodic Stokes problems [64, 58, 42], methods for problems in planar periodicity, e.g. when periodicity is applied to (x, y) and z is “free”, are less so (see e.g. [52, 28]). However, such systems, including wall-confined systems, applications in biology (such as beating flagella in planar configurations [9, 36, 38]), are of growing interest.

The present work deals with the efficient, $\mathcal{O}(N \log N)$, and spectrally accurate summation of Stokes potentials in the 2P setting. To clarify, let $\Omega = [0, L]^3$ and consider Stokes equations for $\mathbf{x} \in \Omega$,

$$\begin{aligned} -\nabla p(\mathbf{x}) + \mu \Delta \mathbf{u}(\mathbf{x}) &= \mathbf{f}(\mathbf{x}) \\ \nabla \cdot \mathbf{u}(\mathbf{x}) &= 0, \end{aligned} \tag{1}$$

where $\mathbf{u}(\mathbf{x})$ denotes the velocity field, $p(\mathbf{x})$ the pressure, and $\mathbf{f}(\mathbf{x})$ the force applied to the fluid. The fundamental solution of Stokes flow represents solutions of the singularly forced Stokes equations, i.e. (1) with $\mathbf{f}(\mathbf{x}) = \mathbf{f}_0 \delta(\mathbf{x} - \mathbf{x}_0)$.

Introducing the *Stokeslet*,

$$S(\mathbf{x}) = \frac{\mathbf{I}}{\|\mathbf{x}\|} + \frac{\mathbf{x} \otimes \mathbf{x}}{\|\mathbf{x}\|^3}, \tag{2}$$

where $(\mathbf{I})_{ij} = \delta_{ij}$ is the identity and $\mathbf{x} \otimes \mathbf{x}$ is the outer product $x_i x_j$, the solution of (1) in free space with $\mathbf{f}(\mathbf{x}) = \mathbf{f}_0 \delta(\mathbf{x} - \mathbf{x}_0)$ can be written:

$$\mathbf{u}(\mathbf{x}) = \frac{1}{8\pi\mu} \int_{\mathbb{R}^3} S(\mathbf{x} - \mathbf{y}) \mathbf{f}_0 \delta(\mathbf{y} - \mathbf{x}_0) d\mathbf{y} = \frac{1}{8\pi\mu} S(\mathbf{x} - \mathbf{x}_0) \mathbf{f}_0.$$

See e.g. the textbook by Pozrikidis [51, p. 22] for a derivation of (2). A solution $\mathbf{u}(\mathbf{x})$, $\mathbf{x} \in \Omega$, that satisfies periodicity is expressed as an infinite sum over periodic images of \mathbf{f}_0 convolved with S , the Stokeslet,

$$\begin{aligned} \mathbf{u}(\mathbf{x}) &= \frac{1}{8\pi\mu} \int_{\mathbb{R}^3} S(\mathbf{x} - \mathbf{y}) \sum_{\mathbf{p} \in \mathbb{Z}^d} \mathbf{f}_0 \delta(\mathbf{y} - \mathbf{x}_n + \tau(\mathbf{p})) d\mathbf{y} \\ &= \frac{1}{8\pi\mu} \sum_{\mathbf{p} \in \mathbb{Z}^d} S(\mathbf{x} - \mathbf{x}_n + \tau(\mathbf{p})) \mathbf{f}_0, \end{aligned}$$

where $d = 1, 2, 3$ is the dimension of periodicity (recall, $\mathbf{x} \in \mathbb{R}^3$ throughout) and $\tau : \mathbb{Z}^d \rightarrow \mathbb{R}^3$ is a translation into the periodic image \mathbf{p} . Under fully periodic boundary conditions (3P) one would let $\tau(\mathbf{p}) = L\mathbf{p}$, and in the 2-periodic (2P) case we let $\tau(\mathbf{p}) = [L\mathbf{p}, 0]$.

In light of the applications surveyed above, we let \mathbf{f} denote an array of point forces,

$$\mathbf{f}(\mathbf{x}) = \sum_{n=1}^N \mathbf{f}_n \delta(\mathbf{x} - \mathbf{x}_n), \quad (3)$$

where \mathbf{f}_n may contain any particular set of e.g. quadrature weights and physical constants. We focus on the evaluation the periodized Stokeslet sum

$$\mathbf{u}(\mathbf{x}) = \sum_{\mathbf{p} \in \mathbb{Z}^d} \sum_{n=1}^N S(\mathbf{x} - \mathbf{x}_n + \tau(\mathbf{p})) \mathbf{f}_n, \quad (4)$$

Note that the terms in (4) decay as $1/r$, and (4) is obviously not absolutely summable. Takemoto et al. [67] discuss this in the related context of the electrostatic potential. However, the practical computation of (4) is plainly infeasible, even for small N , so fast methods are essential. Alternatives exist at this point, including pursuing extensions to the fast multipole method (FMM) by Greengard and Rokhlin [22]. There exist FMMs that incorporate periodicity in 3D, e.g. Kudin & Scuseria [40] for electrostatics, and FMM-related methods for Stokes [19] in 2D with periodicity. However, the dominating framework for periodic problems in this setting incorporates periodicity by using Fourier transforms. The basic principles for how to proceed in that direction have long been clear, neatly divided into two stages:

- (a) Decompose the Stokeslet sum (4) into rapidly converging parts, e.g. by applying ideas from *Ewald summation*.
- (b) Devise a method to reduce the complexity of computing the decomposed Stokeslet sums, e.g. by means of FFT-based methods.

The extent to which this has been realized depends on the periodic structure of the problem. In the fully periodic (3P) setting, various decompositions exist that clarify (a), and methods with $\mathcal{O}(N \log N)$ complexity have been developed (b), as we survey in Section 2.

In the case of planar periodicity (2P), the picture is much less clear. Existing decompositions pertaining to (a) are surveyed in Section 3, after which we derive an Ewald-type sum for computing (4) (Section 3.2). A fast, $\mathcal{O}(N \log N)$, method is presented in Section 4, which, as far as we know, is the first reported method that deals with (b) in the 2-periodic setting.

Interestingly, the fast method we propose (b) is, in some ways, simpler than the underlying Ewald sum (a) that we derive. As shall become clear, this has to do with a relationship between the 2- and 3-periodic settings, which we exploit for the fast method.

We demonstrate several appealing characteristics of the proposed method: spectral accuracy; efficiency in both run-time and memory; clear error estimation and parameter selection; and a close and revealing correspondence to methods for the 3P problem. This will, we hope, facilitate future computational investigations of micro- and complex flow systems, enabling large systems to be simulated accurately.

2 Stokeslet Ewald sum in full periodicity

We start by summarizing well-established results for the fully periodic case. Before interest in solving Stokes equations took off there was already a large body of work established on a related problem in electrostatics – summing Coulomb potentials under periodicity (solving a Poisson problem, rather than Stokes) – known as Ewald summation. The basic principle is that the potential, $\phi \sim 1/r$, is split into a short range part that is exponentially decaying, and a long range part that is very smooth (and thus exponentially convergent in reciprocal space).

Pioneering work by Hasimoto [24] showed that a 3-periodic vector field $\mathbf{u}^{3P}(\mathbf{x})$ can be computed in a Ewald-like manner,

$$\begin{aligned} \mathbf{u}^{3P}(\mathbf{x}_m) = & \sum_{\mathbf{p} \in \mathbb{Z}^3} \sum_{n=1}^N A(\xi, \mathbf{x}_m - \mathbf{x}_n + L\mathbf{p}) \mathbf{f}_n + \\ & + \frac{8\pi}{L^3} \sum_{\mathbf{k} \neq 0} B(\xi, \mathbf{k}) e^{-k^2/4\xi^2} \sum_{n=1}^N \mathbf{f}_n e^{-i\mathbf{k} \cdot (\mathbf{x}_m - \mathbf{x}_n)} - \frac{4\xi}{\sqrt{\pi}} \mathbf{f}_m, \end{aligned} \quad (5)$$

where

$$A(\xi, \mathbf{x}) = 2 \left(\frac{\xi e^{-\xi^2 r^2}}{\sqrt{\pi} r^2} + \frac{\operatorname{erfc}(\xi r)}{2r^3} \right) (r^2 \mathbf{I} + \mathbf{x} \otimes \mathbf{x}) - \frac{4\xi}{\sqrt{\pi}} e^{-\xi^2 r^2} \mathbf{I}, \quad (6)$$

with $r := \|\mathbf{x}\|$, and

$$B(\xi, \mathbf{k}) = \left(1 + \frac{k^2}{4\xi^2} \right) \frac{1}{k^4} (k^2 \mathbf{I} - \mathbf{k} \otimes \mathbf{k}). \quad (7)$$

The parameter $\xi > 0$, which \mathbf{u}^{3P} is independent of, is known as the Ewald parameter and controls the rate at which the two sums converge relative to each other. Note here that the two sums in (5) have the desired structure – the first is a sum in real space that converges roughly as $e^{-\xi^2 r^2}$, and the second is a sum in \mathbf{k} -space that converges as roughly as $e^{-k^2/4\xi^2}$. Other decompositions exist, see Pozrikidis [52, Sec. 3.1, 4.1].

2.1 Fast methods in full periodicity

The $\sim 1/r$ convergence of the original Stokeslet sum (4) is *vastly* improved by the Ewald method (5). However, the complexity of computing the Ewald sum (5) is still severely limiting. There are two reasons for this: First, summing (5) for all \mathbf{x}_m has $\mathcal{O}(N^2)$ complexity. Secondly, the constant hidden in the formal complexity can be *very* large; in fact, it grows cubically with higher accuracy.

Faster methods for the corresponding Poisson problem in electrostatics and molecular simulation have been around for three decades, following work by Hockney & Eastwood [26]; see the survey by Deserno & Holm [12], or recent work by the present authors [44].

Such methods have been adapted for the 3P Stokes Ewald sum (5), starting with Sierou & Brady [64] (embedded in the framework of “Stokesian dynamics”). Their method is based on the *Particle Mesh Ewald* (PME) method by Darden et al. [11]. Saintillan et al. [58], in their method for sedimenting fibers in Stokes flow, base a fast method for the Stokeslet sum on a refinement of the PME method, known as *Smooth Particle Mesh Ewald* (SPME) [14]. The SPME method is known to be more accurate than its predecessor, though still of polynomial order. Recognizing that the exponentially fast convergence of the underlying Ewald sums is lost when a traditional PME approach is used, the present authors presented a spectrally accurate PME-type method for Stokes in [42].

3 2-periodic Stokeslet Ewald sum

Perhaps counter to intuition, one should not expect a method for 2-periodic systems to follow by elementary manipulations of the 3P decomposition (5) – to the contrary, one is best advised to start anew from the Stokeslet sum (4). It is also instructive to review the corresponding transition from 3P to 2P in the electrostatics setting, as we do in [43]. One finds that consolidation, on the level of agreeing on a preferred decomposition, has yet to happen (cf. e.g. the 2P Ewald sum in Gryzbowski et al. [23] and a survey of non-Ewald methods by Mazars [50]), and that fast PME-type methods are considerably less mature than their 3P counterparts, though we hope that [43] contributes in this direction.

There does exist 2P Ewald decompositions for Stokes – notably in Pozrikidis [52], relating to earlier work by Ishii [28]. While it should be emphasized that [52] is among the most valuable references in the present context, we find the results given therein lacking in two respects: First, it turns out to be quite straight-forward to derive and present a 2P Stokes Ewald sum in explicit form, whereas Pozrikidis [52, Sec. 2.2] is content with giving a “generating function” and a differential operator. Secondly, and more importantly, the results on offer in [52] do not, at least to us, suggest how a fast PME-type method could be developed.

Such a fast method being our objective, we now set out to derive a 2P Ewald sum for Stokes in a suitable way. To give an overview, we start by deriving a pure \mathbf{k} -space solution to a 2-periodic Stokes problem that decays as $z \rightarrow \pm\infty$, which we then decompose using the “screening function” (15) proposed by Hernandez-Ortiz et al. [25] to generate the Hasimoto decomposition (5)-(7) in the 3-periodic setting. We then consider the family of solutions obtained by adding a piecewise linear function, showing that this admits an end-result which is differentiable. Under certain conditions, we show that these smooth solutions have finite limits as $z \rightarrow \pm\infty$, as expected physically. The resolution of the smoothness/singularity issue is quite compactly discussed in related work [52, pp. 83-84], [28, p. 676]; this may suit some readers more than others.

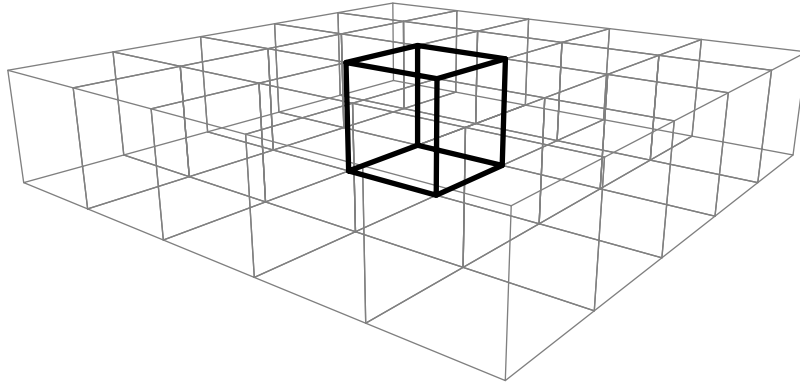


Figure 1: Planar periodicity (2P): Primary cell replicated infinitely in the plane.

3.1 2P Stokeslet Ewald derivation: preliminaries

3.1.1 A mixed Fourier transform

The conventions for Fourier transform pairs used in the present work are given in Appendix B. As in [43], we start with observing that the periodic structure of a 2-periodic function $h(\mathbf{x})$ implies that its spectral representation will be *mixed* in the following sense: Let $h(\mathbf{x}) = h(\rho, z)$ be periodic in the (x, y) -plane and “free” in z , i.e. $\rho := (x, y) \in \Omega = [0, L]^2$ and $z \in \mathbb{R}$. Then a Fourier representation of h is

$$h(\rho, z) = \frac{1}{2\pi} \sum_{\mathbf{k}} \int_{-\infty}^{\infty} \hat{h}(\mathbf{k}, \kappa) e^{i\mathbf{k}\cdot\rho} e^{i\kappa z} d\kappa, \quad (8)$$

where $\mathbf{k} \in 2\pi\mathbb{Z}^2/L$ and $\kappa \in \mathbb{R}$. We shall assume that $h(\rho, z \rightarrow \pm\infty)$ decays faster than any inverse power of z . In this setting, (8) exists. Also under the present assumptions, 2P versions of several familiar results from spectral analysis hold, such as the Poisson summation formula, Parseval/Plancherel’s theorems and the convolution theorem, see [43].

3.1.2 Solution of a 2-periodic Stokes problem

Before we address Ewald summation for the 2P Stokes problem, we need to establish (slowly converging) solutions of the original problem that, crucially, vanishes as $z \rightarrow \pm\infty$. Consider the Stokes equations,

$$\begin{aligned} -\nabla p(\mathbf{x}) + \mu\Delta\mathbf{u}(\mathbf{x}) + \mathbf{f}(\mathbf{x}) &= 0 \\ \nabla \cdot \mathbf{u}(\mathbf{x}) &= 0 \end{aligned}$$

under 2-periodic boundary conditions with respect to Ω . Presently, assume that the source term, \mathbf{f} , has a mixed Fourier transform, $\hat{\mathbf{f}}(\mathbf{k}, \kappa)$, and expand \mathbf{u} and $\mathbf{q} := \nabla p$ likewise,

$$\begin{aligned} \mathbf{u}(\mathbf{x}) = \mathbf{u}(\rho, z) &= \frac{1}{2\pi} \sum_{\mathbf{k}} \int_{\mathbb{R}} \hat{\mathbf{u}}(\mathbf{k}, \kappa) e^{i\mathbf{k}\cdot\rho} e^{i\kappa z} d\kappa \\ \nabla p(\mathbf{x}) = \nabla p(\rho, z) &= \frac{1}{2\pi} \sum_{\mathbf{k}} \int_{\mathbb{R}} \hat{\mathbf{q}}(\mathbf{k}, \kappa) e^{i\mathbf{k}\cdot\rho} e^{i\kappa z} d\kappa. \end{aligned} \quad (9)$$

Inserting into Stokes equations, with $\mathbf{k} := (\mathbf{k}, \kappa) \in \{2\pi\mathbb{Z}^2/L\} \times \mathbb{R}$,

$$\begin{aligned}\hat{\mathbf{q}} + \mu\|\mathbf{k}\|^2\hat{\mathbf{u}} &= \hat{\mathbf{f}} \\ i\mathbf{k} \cdot \hat{\mathbf{u}} &= 0.\end{aligned}$$

As \mathbf{u} should vanish at infinity we may omit summing over $\mathbf{k} = 0$, because $\hat{\mathbf{u}}(0, \kappa) = 0$ is implied. Eliminating the pressure gradient above, $\hat{\mathbf{q}}(\mathbf{k}, \kappa) = (\mathbb{k} \otimes \mathbb{k})\hat{\mathbf{f}}(\mathbf{k}, \kappa)/\|\mathbf{k}\|^2$ (since \mathbf{q} is a gradient $\hat{\mathbf{q}}(\mathbf{k})$ is parallel to \mathbf{k}), gives

$$\hat{\mathbf{u}}(\mathbf{k}) = \hat{\mathbf{u}}(\mathbf{k}, \kappa) = \frac{1}{\mu} \left(\frac{\mathbf{I}}{\|\mathbf{k}\|^2} - \frac{\mathbb{k} \otimes \mathbb{k}}{\|\mathbf{k}\|^4} \right) \hat{\mathbf{f}}(\mathbf{k}, \kappa), \quad \mathbf{k} \neq 0. \quad (10)$$

Hence, in light of (9),

$$\mathbf{u}(\rho, z) = \frac{1}{2\pi\mu} \sum_{\mathbf{k} \neq 0} \int_{\mathbb{R}} \left(\frac{\mathbf{I}}{\|\mathbf{k}\|^2} - \frac{\mathbb{k} \otimes \mathbb{k}}{\|\mathbf{k}\|^4} \right) \hat{\mathbf{f}}(\mathbf{k}, \kappa) e^{i\mathbf{k} \cdot \rho} e^{i\kappa z} d\kappa. \quad (11)$$

Recalling $\mathbf{f}(\mathbf{x})$ from (3), we absorb a factor $8\pi\mu$ into the coefficients \mathbf{f}_n for convenience and conformity with convention. With that, (11) becomes

$$\tilde{\mathbf{u}}(\rho, z) = \frac{4}{L^2} \sum_{\mathbf{k} \neq 0} \int_{\mathbb{R}} \left(\frac{\mathbf{I}}{\|\mathbf{k}\|^2} - \frac{\mathbb{k} \otimes \mathbb{k}}{\|\mathbf{k}\|^4} \right) \sum_{n=1}^N \mathbf{f}_n e^{i\mathbf{k} \cdot (\rho - \rho_n)} e^{i\kappa(z - z_n)} d\kappa,$$

where the integrals are computable. We obtain (see Appendix A.1):

$$\tilde{\mathbf{u}}(\rho, z) = \frac{4}{L^2} \sum_{\mathbf{k} \neq 0} \sum_{n=1}^N \tilde{Q}(\mathbf{k}, z - z_n) \mathbf{f}_n e^{i\mathbf{k} \cdot (\rho - \rho_n)}, \quad (12)$$

where

$$\tilde{Q}(\mathbf{k}, z) = \frac{e^{-\|\mathbf{k}\||z|}}{\|\mathbf{k}\|} \begin{bmatrix} \pi - \frac{(\pi\|\mathbf{k}\||z| + \pi)k_1^2}{2\|\mathbf{k}\|^2} & -\frac{\pi(\|\mathbf{k}\||z| + 1)k_1 k_2}{2\|\mathbf{k}\|^2} & -\frac{1}{2}i\pi z k_1 \\ -\frac{\pi(\|\mathbf{k}\||z| + 1)k_1 k_2}{2\|\mathbf{k}\|^2} & \pi - \frac{(\pi\|\mathbf{k}\||z| + \pi)k_2^2}{2\|\mathbf{k}\|^2} & -\frac{1}{2}i\pi z k_2 \\ -\frac{1}{2}i\pi z k_1 & -\frac{1}{2}i\pi z k_2 & \frac{1}{2}(\pi\|\mathbf{k}\||z| + \pi) \end{bmatrix}. \quad (13)$$

Note that $\tilde{\mathbf{u}}$ is well-defined, but, as will be discussed in Section 3.2.2, fails to be differentiable in an (x, y) -plane around each z_n .

3.2 2P Stokeslet Ewald derivation

A fruitful and flexible approach to deriving Ewald sums is to compute convolutions of source term with a so called screening function – this is the classical approach for the 3P Laplace (electrostatics) problem. In planar periodicity the singularities encountered are more severe, and the appropriate behavior in the limit $z \rightarrow \pm\infty$ not as straight forward as the corresponding “tin foil” (or, for Stokes, “pressure gradient counters net force”) conditions that enter 3P derivations. Our approach here is to construct a decomposition of (12) and then address the regularity issue.

By “screening function” we mean any normalized function, $\|\gamma(\mathbf{x})\|_2 = 1$, that decays smoothly away from zero, such that a decomposition,

$$\mathbf{f}(\mathbf{x}) = ((\delta - \gamma) * \mathbf{f})(\mathbf{x}) + (\gamma * \mathbf{f})(\mathbf{x}) = \mathbf{f}(\mathbf{x}) - \mathbf{f}_\gamma(\mathbf{x}) + \mathbf{f}_\gamma(\mathbf{x}),$$

where $\delta(\mathbf{x})$ denotes the Dirac measure on \mathbb{R}^3 and $\mathbf{f}_\gamma(\mathbf{x}) := (\mathbf{f} * \gamma)(\mathbf{x})$, is well defined. With this, clearly,

$$\mathbf{u}(\mathbf{x}) = \frac{1}{8\pi\mu} \int_{\mathbb{R}^3} S(\mathbf{x} - \mathbf{y}) (\mathbf{f}(\mathbf{y}) - \mathbf{f}_\gamma(\mathbf{y})) d\mathbf{y} + \frac{1}{8\pi\mu} \int_{\mathbb{R}^3} S(\mathbf{x} - \mathbf{y}) \mathbf{f}_\gamma(\mathbf{y}) d\mathbf{y}. \quad (14)$$

As noted, the standard derivation for the 3P Laplace case is to take γ as a pure Gaussian, compute the first convolution directly and treat the second term in reciprocal space. Interestingly, in a short paper sparse on details [25], Hernandez-Ortiz et al. give a screening function,

$$\gamma(r) = \frac{\xi^3}{\sqrt{\pi^3}} e^{-\xi^2 r^2} \left(\frac{5}{2} - \xi^2 r^2 \right), \quad (15)$$

that generates exactly the 3P Hasimoto decomposition (5)-(7).

3.2.1 The real-space sum

The first term in (14) can be computed directly, as is standard in this context (though the calculations are laborious), and one finds that

$$\int_{\mathbb{R}^3} S(\mathbf{x} - \mathbf{y}) (\mathbf{f}(\mathbf{y}) - \mathbf{f}_\gamma(\mathbf{y})) d\mathbf{y} = \sum_{n=1}^N \sum_{\mathbf{p} \in \mathbb{Z}^2} A(\xi, \mathbf{x} - \mathbf{x}_n + L\mathbf{p}) \mathbf{f}_n, \quad (16)$$

where A is the same (though summed over a two-dimensional lattice this time) *vis-a-vis* the 3P decomposition (6).

Note that a particle does not itself contribute to the potential field, or flow, it experiences, so it is natural to simply drop the term in (16) that corresponds to $\mathbf{p} = 0$ when $m = n$. However, by the decomposition (14), part of the contribution that we're trying to remove has gone into the second term. By computing the difference between the free space Stokeslet and the real-space term, we can find this contribution. This is to be subtracted off, so we do it with the opposite sign:

$$\lim_{\|\mathbf{x}\| \rightarrow 0} (A(\mathbf{x}, \xi) - S(\mathbf{x})) = \lim_{\|\mathbf{x}\| \rightarrow 0} \left(-(\alpha + \operatorname{erf}(\xi\|\mathbf{x}\|)) \frac{\mathbf{I}}{\|\mathbf{x}\|} + (\alpha - \operatorname{erf}(\xi\|\mathbf{x}\|)) \frac{\mathbf{x} \otimes \mathbf{x}}{\|\mathbf{x}\|^3} \right) = -\frac{4\xi}{\sqrt{\pi}} \mathbf{I},$$

where $\alpha := 2\xi\pi^{-1/2}\|\mathbf{x}\|e^{-\xi^2\|\mathbf{x}\|^2}$. By convention, this term is denoted ‘‘self interaction’’ which can lead to some confusion, since it's the term removing self interaction that is included in the \mathbf{k} -space sum. Nonetheless, we have arrived at two parts of the 2P Stokeslet Ewald sum,

$$\mathbf{u}^R(\mathbf{x}_m) := \sum_{n=1}^N \sum_{\mathbf{p} \in \mathbb{Z}^2}^* A(\xi, \mathbf{x}_m - \mathbf{x}_n + L\mathbf{p}) \mathbf{f}_n \quad (17)$$

$$\mathbf{u}_{\text{self}}(\mathbf{x}_m) := -\frac{4\xi}{\sqrt{\pi}} \mathbf{f}_m. \quad (18)$$

The notational inconvenience $*$, signifying the omission of the term $\{\mathbf{p} = 0, n = m\}$ in (17), is standard.

3.2.2 The \mathbf{k} -space sum

Turning to the second term in the Stokeslet decomposition (14), first note that both terms in (14) are solutions to Stokes equations. Moreover, both \mathbf{f}_γ and $\mathbf{f} - \mathbf{f}_\gamma$ are admissible under the assumptions of Section 3.1.2. The Fourier transform of γ over \mathbb{R}^3 is

$$\hat{\gamma}(\mathbf{k}) = \left(1 + \frac{k^2}{4\xi^2}\right) e^{-k^2/4\xi^2}.$$

In light of (11) we let $\mathbf{f}_\gamma = \mathbf{f} * \gamma$ generate a function \mathbf{u}^F that satisfies $\mathbf{u}^F \rightarrow 0$ as $z \rightarrow \pm\infty$,

$$\begin{aligned} \mathbf{u}^F(\rho, z) &= \frac{1}{2\pi\mu} \sum_{\mathbf{k} \neq 0} \int_{\mathbb{R}} \left(\frac{\mathbf{I}}{\|\mathbf{k}\|^2} - \frac{\mathbf{k} \otimes \mathbf{k}}{\|\mathbf{k}\|^4} \right) \hat{\mathbf{f}}_\gamma(\mathbf{k}, \kappa) e^{i\mathbf{k} \cdot \rho} e^{i\kappa z} d\kappa \\ &= \frac{4}{L^2} \sum_{\mathbf{k} \neq 0} \int_{\mathbb{R}} \left(\frac{\mathbf{I}}{\|\mathbf{k}\|^2} - \frac{\mathbf{k} \otimes \mathbf{k}}{\|\mathbf{k}\|^4} \right) \left(1 + \frac{\|\mathbf{k}\|^2}{4\xi^2}\right) e^{-\|\mathbf{k}\|^2/4\xi^2} \sum_{n=1}^N f_n e^{i\mathbf{k} \cdot (\rho - \rho_n)} e^{i\kappa(z - z_n)} d\kappa \\ &= \frac{4}{L^2} \sum_{\mathbf{k} \neq 0} \int_{\mathbb{R}} B(\mathbf{k}) e^{-\|\mathbf{k}\|^2/4\xi^2} \sum_{n=1}^N \mathbf{f}_n e^{i\mathbf{k} \cdot (\rho - \rho_n)} e^{i\kappa(z - z_n)} d\kappa, \end{aligned} \quad (19)$$

where we have used Poisson summation and grouped similar Fourier coefficients.

For future reference, we note that this expression is the starting point from which we develop a fast PME-type method. Given the present mixed periodic setting, the close correspondence between (19) and (7) is entirely expected, and illuminating *per se*.

As it transpires in Appendix A.2, the integrals above,

$$Q(\mathbf{k}, z) := e^{-\|\mathbf{k}\|^2/4\xi^2} \int_{\mathbb{R}} \left(\frac{\mathbf{I}}{\|\mathbf{k}\|^2} - \frac{\mathbf{k} \otimes \mathbf{k}}{\|\mathbf{k}\|^4} \right) \left(1 + \frac{\|\mathbf{k}\|^2}{4\xi^2}\right) e^{-\kappa^2/4\xi^2} e^{i\kappa z} d\kappa, \quad (20)$$

can be computed. For clarity of notation it is useful to let

$$Q(\mathbf{k}, z) = Q^{\mathbf{I}}(\mathbf{k}, z) + Q^{\mathbf{k} \otimes \mathbf{k}}(\mathbf{k}, z),$$

where the meaning of the superscripts is implied from the terms in the first factor under the integral in (20). With this, and the computations in Appendix A.2, it follows that we may write \mathbf{u}^F as a sum,

$$\begin{aligned} \mathbf{u}^F(\rho_m, z_m) &= \frac{4}{L^2} \sum_{\mathbf{k} \neq 0} \sum_{n=1}^N \left((Q^{\mathbf{I}}(\mathbf{k}, z_{mn}) + \operatorname{Re} Q^{\mathbf{k} \otimes \mathbf{k}}(\mathbf{k}, z_{mn})) \cos(\mathbf{k} \cdot \rho_{mn}) - \right. \\ &\quad \left. + \operatorname{Im} Q^{\mathbf{k} \otimes \mathbf{k}}(\mathbf{k}, z_{mn}) \sin(\mathbf{k} \cdot \rho_{mn}) \right) \mathbf{f}_n, \end{aligned} \quad (21)$$

where

$$Q^{\mathbf{I}}(\mathbf{k}, z) = 2 \left(\frac{J_0^0(z)}{4\xi^2} + J_0^1(\|\mathbf{k}\|, z) \right) \mathbf{I} \quad (22)$$

and

$$Q^{\mathbf{k} \otimes \mathbf{k}}(\mathbf{k}, z) = -2 \begin{bmatrix} k_1^2 \left(\frac{J_1^0}{4\xi^2} + J_2^0 \right) & k_1 k_2 \left(\frac{J_1^0}{4\xi^2} + J_2^0 \right) & k_1 \left(\frac{iK_1^1}{4\xi^2} + iK_2^1 \right) \\ k_1 k_2 \left(\frac{J_1^0}{4\xi^2} + J_2^0 \right) & k_2^2 \left(\frac{J_1^0}{4\xi^2} + J_2^0 \right) & k_2 \left(\frac{iK_1^1}{4\xi^2} + iK_2^1 \right) \\ k_1 \left(\frac{iK_1^1}{4\xi^2} + iK_2^1 \right) & k_2 \left(\frac{iK_1^1}{4\xi^2} + iK_2^1 \right) & \frac{J_1^2}{4\xi^2} + J_2^2 \end{bmatrix} (\|\mathbf{k}\|, z). \quad (23)$$

The terms J_q^p and K_q^p are short-hand for the various scalar integrals that can be identified by studying the integrand in Q . With

$$\lambda := e^{-k^2/4\xi^2 - \xi^2 z^2} \quad (24)$$

$$\theta_+ := e^{kz} \operatorname{erfc} \left(\frac{k}{2\xi} + \xi z \right) \quad (25)$$

$$\theta_- := e^{-kz} \operatorname{erfc} \left(\frac{k}{2\xi} - \xi z \right) \quad (26)$$

we can write down the computed integrals as

$$J_0^0(z, k) = \sqrt{\pi} \lambda \xi \quad (27)$$

$$J_1^0(z, k) = \frac{\pi(\theta_- + \theta_+)}{4k} \quad (28)$$

$$J_2^0(z, k) = \frac{\sqrt{\pi} \lambda}{4k^2 \xi} + \pi \left(\frac{\theta_- + \theta_+}{8k^3} + \frac{(\theta_- - \theta_+)z}{8k^2} - \frac{\theta_- + \theta_+}{16k\xi^2} \right) \quad (29)$$

$$J_1^2(z, k) = \frac{1}{4} \pi (-\theta_- - \theta_+) k + \sqrt{\pi} \lambda \xi \quad (30)$$

$$J_2^2(z, k) = \pi \left(\frac{(\theta_- + \theta_+)k}{16\xi^2} + \frac{\theta_- + \theta_+}{8k} + \frac{1}{8}(\theta_+ - \theta_-)z \right) - \frac{\sqrt{\pi} \lambda}{4\xi} \quad (31)$$

$$K_1^1(z, k) = \frac{\pi(\theta_- - \theta_+)}{4} \quad (32)$$

$$K_2^1(z, k) = \pi \left(\frac{\theta_+ - \theta_-}{16\xi^2} + \frac{(\theta_- + \theta_+)z}{8k} \right). \quad (33)$$

Despite some difficulty of notation, the sum (21) is straight-forward to evaluate.

Now, recall that we are presently aiming for a decomposition of the pure \mathbf{k} -space solution (12), wherein the $\mathbf{k} = 0$ term was dropped to ensure decay as $z \rightarrow \pm\infty$. However, by the decomposition (14), part of the $\mathbf{k} = 0$ mode has gone into the real-space sum (17) and must be subtracted off. Computing (12) explicitly has provided a \mathbf{k} -space view of the real-space sum, so that the term to be removed can be extracted as

$$\mathbf{u}^*(z) = \lim_{\mathbf{k} \rightarrow 0} \left(\hat{\mathbf{u}}(\mathbf{k}) - \hat{\mathbf{u}}^F(\mathbf{k}) \right) = \lim_{\mathbf{k} \rightarrow 0} \frac{4}{L^2} \left(\sum_{n=1}^N (\tilde{Q}(\mathbf{k}, z - z_n) - Q(\mathbf{k}, z - z_n)) \mathbf{f}_n \right).$$

Computing the desired limit, one finds

$$\lim_{\mathbf{k} \rightarrow 0} \left(Q(\mathbf{k}, z) - \tilde{Q}(\mathbf{k}, z) \right) = \begin{pmatrix} a(z) & 0 & 0 \\ 0 & a(z) & 0 \\ 0 & 0 & 0 \end{pmatrix},$$

where

$$a(z) := \pi|z| - \pi z \operatorname{erf}(z\xi) - \frac{e^{-z^2\xi^2}\sqrt{\pi}}{2\xi}, \quad (34)$$

so that

$$\mathbf{u}^*(z) = \frac{4}{L^2} \sum_{n=1}^N a(z - z_n) \mathbf{I}_2 \mathbf{f}_n, \quad \mathbf{I}_2 := \begin{bmatrix} 1 & 0 & 0 \\ 0 & 1 & 0 \\ 0 & 0 & 0 \end{bmatrix}.$$

We now have the desired decomposition of (12),

$$\tilde{\mathbf{u}}(\rho_m, z_m) = \mathbf{u}^R(\rho_m, z_m) + \mathbf{u}^F(\rho_m, z_m) - \mathbf{u}^*(z_m) + \mathbf{u}_{\text{self}}.$$

Naturally, the non-smoothness in (12) is present here (in the term \mathbf{u}^*). However, we can recover a smooth solution by relaxing the restriction that $\mathbf{u} \rightarrow 0$ as $z \rightarrow \pm\infty$. To any \mathbf{u} that satisfies the Stokes equation (1) we can add a linear function. By that token, and in close analogy to how the 2P Ewald sum for electrostatics was obtained in [43], we subtract a piecewise linear function,

$$\begin{aligned} \mathbf{u}^{F,\mathbf{k}=0}(\mathbf{x}_m) &= -\frac{4\pi}{L^2} \sum_{n=1}^N |z_m - z_n| \mathbf{I}_2 \mathbf{f}_n - \mathbf{u}^* \\ &= -\frac{4}{L^2} \sum_{n=1}^N \left(\pi(z_m - z_n) \operatorname{erf}((z_m - z_n)\xi) + \frac{\sqrt{\pi}}{2\xi} e^{-(z_m - z_n)^2 \xi^2} \right) \mathbf{I}_2 \mathbf{f}_n. \end{aligned} \quad (35)$$

With this, the derivation of the 2P Stokes Ewald sum is complete. We have that

$$\mathbf{u}(\mathbf{x}_m) = \mathbf{u}(\rho_m, z_m) = \mathbf{u}^R(\rho_m, z_m) + \mathbf{u}^F(\rho_m, z_m) + \mathbf{u}^{F,\mathbf{k}=0}(z_m) + \mathbf{u}_{\text{self}}, \quad (36)$$

from (17), (21), (35) and (18). These are nice and exponentially convergent sums, but, as discussed in the introduction, the complexity of evaluating them for a large system is debilitating. Note that $\mathbf{u}^{F,\mathbf{k}=0}$ contains terms that look like an unbounded shear flow in z . However, if the coefficients \mathbf{f}_n sum to zero in the first two components, $\mathbf{u}^{F,\mathbf{k}=0}$ tends to finite limits as $z \rightarrow \pm\infty$. As in the electrostatics case, one can show that

$$\left(\lim_{z \rightarrow \infty} \mathbf{u}(\rho, z) - \lim_{z \rightarrow -\infty} \mathbf{u}(\rho, z) \right) = \frac{8\pi}{L^2} \sum_{n=1}^N z_n \mathbf{f}_n \mathbf{I}_2, \quad \text{if } \sum_{n=1}^N (\mathbf{f}_n)_j = 0, \quad j = 1, 2.$$

That is, in the planar directions (x, y) the flow sees a transition (across $z \in (0, L)$ continuously) proportional to the dipole moment in z .

3.3 Truncation error estimates for 2P Stokeslet Ewald sums

It's noteworthy that the usefulness of Ewald sums (cf. Section 4.4, on parameter selection) rests on the availability of truncation error estimates. Therefore, we need to endow the 2P Stokeslet Ewald sums, (17) and (21), with such estimates.

To this end, let the real-space sum (17) be truncated such that only interactions between particles (including periodic images) within a distance r_c from each other are included. That is, let

$$\mathbf{u}_{r_c}^R(\mathbf{x}_m) := \sum_{n=1}^N \sum_{\mathbf{p} \in \mathbb{Z}^2}^* \mathbf{1}_{r_c}(\|\mathbf{x}_m - \mathbf{x}_n + \tau(\mathbf{p})\|) A(\xi, \mathbf{x}_m - \mathbf{x}_n + \tau(\mathbf{p})) \mathbf{f}_n,$$

where $\mathbf{1}_{r_c}(r)$ denotes the indicator function which is one if $r \leq r_c$ and zero otherwise. Estimating $\|\mathbf{u}^R - \mathbf{u}_{r_c}^R\|$ is most tractable in the RMS norm,

$$e_{\text{rms}} := \sqrt{\frac{1}{N} \sum_{n=1}^N (\mathbf{u}(\mathbf{x}_n) - \mathbf{u}_*(\mathbf{x}_n))^2}. \quad (37)$$

In the electrostatic case, Kolafa & Perram [39] have derived famous truncation error estimates for randomly scattered particles in RMS norm. However, the diagonal terms in A are $A_{jj} = \text{erfc}(\xi r)/r - 2\xi \exp(-\xi^2 r^2)/\sqrt{\pi}$, whereas in the Laplace case only the former (and smaller) term is present. On the other hand, if we disregard the off-diagonal terms in A , the key step in [39, Appendix A, Eq. (14)] becomes tractable for the Stokeslet, and we get estimates for components $j = 1, 2, 3$,

$$\begin{aligned} (e_{\text{rms},j}^R)^2 &\approx \frac{Q_j}{L^3} \int_0^{2\pi} \int_0^\pi \int_{r_c}^\infty A_{jj}^2 r^2 \sin(\theta) dr d\theta d\phi \\ &= \frac{Q_j}{L^3} \left(4r_c \left(e^{-2\xi^2 r_c^2} - \pi \text{erfc}(\xi r_c)^2 \right) + \frac{\sqrt{2\pi}}{\xi} \text{erfc}(\sqrt{2}\xi r_c) \right), \end{aligned} \quad (38)$$

where $Q_j := \sum_{n=1}^N (f_j)_n^2$. In what follows, we suppress the vector index j .

The *estimate* (38) is to be treated as such – it does not include the full operator and it is statistical, the latter meaning that it's only valid if \mathbf{x}_m is randomly distributed. None the less, (38) is very predictive within its domain, as we illustrate in Figure 2. Here we have $N = 10000$, \mathbf{x}_m randomly from a uniform distribution over $\Omega = [0, 1]^3$, \mathbf{f}_m from a uniform distribution centered at zero and the RMS average was formed over 30 random \mathbf{x}_m . Finally, for selecting parameters one would ideally like to solve $e_{\text{rms}}^R(\xi) = \varepsilon$ for ξ , but this does not appear tractable. Rather, we series expand the error estimate for large ξr_c , obtaining that

$$e_{\text{rms}}^R \approx 2 \sqrt{\frac{Q r_c}{L^3}} e^{-\xi^2 r_c^2}, \quad (39)$$

and consequently, assuming that $r_c \geq L^3 \varepsilon^2 / (4Q)$,

$$\xi(r_c, \varepsilon) \approx \frac{1}{r_c} \sqrt{\log \left(\frac{2}{\varepsilon} \sqrt{\frac{Q r_c}{L^3}} \right)}.$$

The agreement between computed errors and the simplified estimate (39) is illustrated in Figure 2.

For the \mathbf{k} -space sum (21), truncated as $\|\mathbf{k}\| \leq 2\pi k_\infty / L$, it's harder to follow Kolafa & Perram [39] and derive a corresponding estimate. Rather than to ignore the issue altogether,

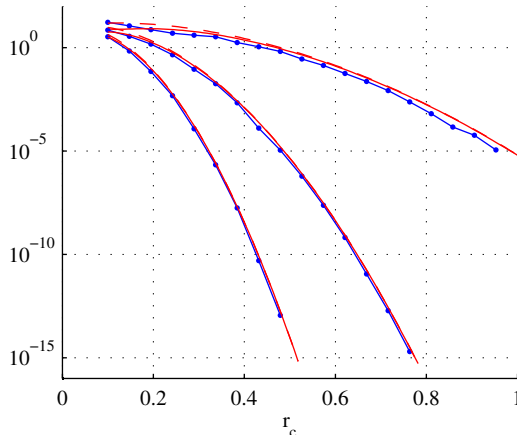


Figure 2: Real-space sum truncation error (37) and estimate (38) of x -component, in RMS-norm, as a function of truncation radius. $N = 10000$, $\Omega = [0, 1]^3$, $\xi = 4, 8, 12$ (top to bottom). As dashed, simplified estimate (39), hardly distinguishable.

which would break the way parameters are selected (cf. Section 4.4), we take a heuristic approach. Based on existing results in the RMS setting, it's natural to suppose that an estimate of the form $e_{\text{rms}}^F \approx C\sqrt{Q}k_\infty^a \xi^b e^{-(\frac{\pi k_\infty}{\xi L})^2}$, for particular a, b , can be of value. A few trial runs quite clearly suggest that good agreement is obtained if $a = -3/2$ and $b = 3$. Moreover, we let $C = L^2\pi^{-4}$, obtaining a heuristic, or practical, error estimate for the truncation error of the \mathbf{k} -space sum (21),

$$e_{\text{rms}}^F \approx \sqrt{Q} \frac{\xi^3 L^2}{\pi^4 k_\infty^{3/2}} e^{-(\frac{\pi k_\infty}{\xi L})^2}. \quad (40)$$

In Figure 3 we give results that demonstrate that this estimate captures the truncation error well for a range of parameters. Here, $\xi = 4, 8, 12$ and $L = 1, 3$, $N = 400, 200$ and the RMS-average is formed over a random set of 30 points¹. We observe satisfying agreement, and, as appropriate, that the estimate is somewhat conservative.

Pertaining to both the real- and \mathbf{k} -space sums, the RMS measure will underestimate errors if particles are not randomly scattered. In that case, it becomes appropriate to consider ∞ -norm estimates. The essential property, that the sums converge at least as fast as $\exp(-r_c^2 \xi^2)$ and $\exp(-(\pi k_\infty / (\xi L))^2)$ respectively, still holds, though obtaining reliable estimates with detailed constants, as in the RMS case, is bound to pose a challenge.

4 Fast methods for 2P Stokes Ewald sums

In Section 2.1 we briefly surveyed fast, $\mathcal{O}(N \log N)$, methods for the fully periodic (3P) problem, and we shall adhere to same framework under 2P:

- a) The real-space sum (17) can be made arbitrarily cheap to compute by choosing the Ewald parameter, ξ , sufficiently large (cf. Section 4.1);

¹The small systems used to evaluate the estimate (40) are small – limited by the computational cost of evaluating (21) for large ξ .

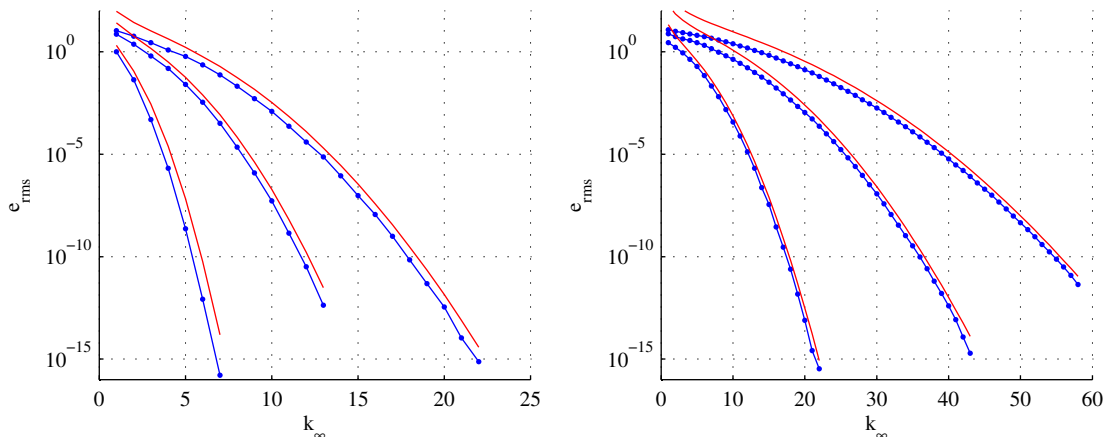


Figure 3: Truncation error of \mathbf{k} -space 2P Stokeslet Ewald sum (21) in RMS norm (37) vs. number of modes k_∞ , i.e. $\|\mathbf{k}\| \leq 2\pi k_\infty/L$. Left: $L = 1, N = 400$. Right: $L = 3, N = 200$. In both panels, $\xi = 4, 8, 12$ (left to right), and (solid line) heuristic error estimate (40).

- b) by using fast Fourier transform (FFT), the (non-singular) \mathbf{k} -space sum (21) can be evaluated in linear time (independently of ξ);
- c) the (2P-only) singularity contribution (35) is easily dealt with as a one-dimensional interpolation problem.

It is really item (b) that is the heart of the matter, that and the glue that hold the parts together: parameter estimation. In the 3P setting one starts from the Ewald sum (the second term in (5), in the Stokes case), and the steps to obtain a fast, FFT-based, method are quite intuitive. That is not to say that the matter is simple; a rather large debt of insight is owed to the early pioneers in the field, such as Hockney & Eastwood [26] and Darden et al. [11].

Attempts to do the same thing in planar periodicity immediately run aground on the algebraic structure of the corresponding \mathbf{k} -space Ewald sum (21) (cf. e.g. Grzybowski et al. [23] for Laplace). Looking at the \mathbf{k} -space 2P Stokes Ewald sum, and its constituent expressions, (21)-(33), it is not hard appreciate the challenge in finding transforms and approximations that mimic the 3P approach. In the electrostatics setting, a variety of non-Ewald (cf. Mazars [50]) and non-2P Ewald methods (cf. Arnold et al. [2] and the references therein), have been developed instead. These methods have not been adapted to Stokes (i.e. deriving corresponding *Lekner sums* [50] or correction terms [2]), and it is quite evident that, at best, a substantial effort would be required to do so.

What we propose, in contrast, starts from the mixed sum/integral (19). Formulating a FFT-based (PME) method becomes a quite straight-forward matter. It follows the same line of reasoning that we set forth in [43]. First, however, we give a few remarks regarding item (a).

4.1 Real-space summation in linear time

The truncated real-space sum

$$\mathbf{u}_{r_c}^R(\mathbf{x}_m) = \sum_{n=1}^N \sum_{\mathbf{p} \in \mathbb{Z}^2}^* \mathbf{1}_{r_c}(\|\mathbf{x}_m - \mathbf{x}_n + \tau(\mathbf{p})\|) A(\xi, \mathbf{x}_m - \mathbf{x}_n + L\mathbf{p}) \mathbf{f}_n,$$

with

$$A(\xi, \mathbf{x}) = 2 \left(\frac{\xi e^{-\xi^2 r^2}}{\sqrt{\pi} r^2} + \frac{\operatorname{erfc}(\xi r)}{2r^3} \right) (r^2 \mathbf{I} + \mathbf{x} \otimes \mathbf{x}) - \frac{4\xi}{\sqrt{\pi}} e^{-\xi^2 r^2} \mathbf{I},$$

is, in order to benefit from much related work, most conveniently written as

$$\mathbf{u}_{r_c}^R(\mathbf{x}_m) = \sum_{\mathbf{y} \in \text{NL}_m} A(\xi, \mathbf{x}_m - \mathbf{y}) \mathbf{f}(\mathbf{y}), \quad (41)$$

where $\text{NL}_m = \text{NL}_m(r_c)$ denotes the set of near neighbors to \mathbf{x}_m (counting periodic images, if necessary). The point being that if $|\text{NL}_m|$ is constant, for all m , as N , the number of sources, grows, then evaluating (41) for all \mathbf{x}_m has complexity $\mathcal{O}(N)$ instead of $\mathcal{O}(N^2)$. This presupposes that all neighbor lists NL_m can be found in linear time, which is the case. In fact, it is quite elementary and we refer the reader to the textbook by Frenkel & Smit [15, Appendix F], and the recent paper [44] by the present authors where additional details are given.

Note that each neighbor list, NL_m , can be viewed as the non-zero pattern for a row in a sparse matrix. In light of this, it's natural to suggest that the evaluation of (41) for all \mathbf{x}_m be implemented as a sparse matrix-vector product, $\mathbf{u}^R \leftarrow \tilde{A}(r_c, \{\mathbf{x}_m\}) \text{vec}(\mathbf{f})$. The $3N \times 3N$ matrix \tilde{A} has a 3×3 block structure corresponding to Cartesian components A_{ij} , but each block has the same sparsity pattern. If (41) is to be evaluated for many \mathbf{f} , as is the case in the context of iterative solution of boundary integral equations (cf. Section 5.1), the matrix form saves a very large amount of redundant arithmetic [58]. In a setting where locations \mathbf{x}_m change, as in fiber simulations [68], the matrix elements of \tilde{A} have to be recomputed, but the sparsity pattern can be valid for several time steps².

4.2 SE2P Stokes: Fast k-space method

The fast method that we give here is based on earlier work by the present authors [42, 44, 43], and this exposition is somewhat condensed and, in contrast to our previous work, draws in its structure and notation from the elegant treatment of the 3P electrostatics case by Shan et al. [60].

Instead of starting from the 2P \mathbf{k} -space Stokes Ewald (21), we invoke the mixed sum-integral form (19)

$$\mathbf{u}^F(\rho_m, z_m) = \frac{4}{L^2} \sum_{\mathbf{k} \neq 0} \int_{\mathbb{R}} B(\mathbb{k}) e^{-\|\mathbf{k}\|^2/4\xi^2} \sum_{n=1}^N \mathbf{f}_n e^{i\mathbf{k} \cdot (\rho - \rho_n)} e^{i\kappa(z - z_n)} d\kappa.$$

²Typically, the neighbor lists NL_m are constructed with some margin, $\|\mathbf{x} - \mathbf{y}\| \leq r_c + r'$, to allow particles to move a distance r' before the neighbor list has to be recomputed.

It is fairly easy [43] to show that $\mathbf{u}^F(\mathbf{x}_m)$ can be obtained as a convolution of a particular smooth function, $\psi : \Omega \times \mathbb{R} \rightarrow \mathbb{R}^3$, with a suitably scaled Gaussian centered in \mathbf{x}_m ,

$$\mathbf{u}^F(\rho_m, z_m) = C' \int_{\mathbb{R}} \int_{\Omega} \psi(\rho, z) e^{-\beta \|\rho - \rho_m\|_*^2} e^{-\beta |z - z_m|^2} d\rho dz, \quad (42)$$

where

$$C' = \left(\frac{2\xi^2}{\pi\eta} \right)^{3/2}, \quad \beta = \frac{2\xi^2}{\eta}$$

and $\eta > 0$ is a parameter. To define ψ , and show how it enters, we recall the decomposition (14) and note that we can view $B(\mathbb{k})e^{-\|\mathbb{k}\|^2/4\xi^2}$ as the \mathbf{k} -space representation of the “regularized” Stokeslet $(S * \gamma)(\mathbf{x})$, as discussed at the outset of Section 3.2. In Section 3.2.2 we proceeded to obtain the Ewald sum (21) by convolving $S * \gamma$ with $\mathbf{f}(\mathbf{x})$ and laboring over the resulting integrals (the convolution itself was trivial though). Mesh-based Ewald methods deviate at this point. The logic is to consider not \mathbf{f} but a regularization, $\mathbf{f}_\eta(\mathbf{x}) = (G(\eta) * \mathbf{f})(\mathbf{x})$, and adjust the Green’s function accordingly. That is, choose a kernel G and determine a modified Green’s function, \tilde{B} , such that

$$\mathbf{u}_\gamma = (S * \gamma(\xi) * \mathbf{f})(\mathbf{x}) = (\mathbf{f} * G(\eta) * \tilde{B} * G(\eta))(\mathbf{x}). \quad (43)$$

It turns out to be advantageous [44] to let $G = C'e^{-\beta\|\mathbf{x}\|^2}$, so that,

$$\mathbf{f}_\eta(\rho, z) = C' \sum_{n=1}^N e^{-\beta \|\rho - \rho_m\|_*^2} e^{-\beta |z - z_m|^2} \mathbf{f}_n, \quad (44)$$

by which its modified Green’s function, $\tilde{B} = e^{-(1-\eta)\|\mathbb{k}\|^2/4\xi^2} B(\mathbf{k}, \kappa)$, follows. The convolution $\mathbf{f}_\eta * \tilde{B}$ is conveniently computed as a multiplication in frequency domain,

$$\hat{\psi}(\mathbf{k}, \kappa) = \begin{cases} 0, & \mathbf{k} = 0 \\ e^{-(1-\eta)(k^2 + \kappa^2)/4\xi^2} B(\mathbf{k}, \kappa) \hat{\mathbf{f}}_\eta(\mathbf{k}, \kappa), & \text{otherwise} \end{cases}. \quad (45)$$

The last convolution in (43), $(\psi * G(\eta))(\mathbf{x})$, brings us back to (42). In [42, 44, 43] detailed and constructive derivations are given instead of this sketch. To clarify, we give a few remarks, starting with a summary of the method:

Summary of method

To compute the (non-singular) \mathbf{k} -space contribution $\mathbf{u}^F(\mathbf{x}_m)$ for all m the steps are as follows: (i) evaluate \mathbf{f}_η (44) on a uniform grid over Ω ; (ii) compute a mixed Fourier transform to arrive at $\hat{\mathbf{f}}_\eta$; (iii) multiply with modified Green’s function according to (45); (iv) an inverse mixed transform yields ψ on a regular grid, so that; (v) the convolution (42) can be computed for all \mathbf{x}_m . In steps (i) and (v), the Gaussians are truncated to have support on P^3 grid points, for some P determined by the acceptable approximation error.

Fast transforms; uniform grids PME-methods become efficient by requiring that the regularized charge distribution $\mathbf{f}_\eta(\mathbf{x})$ be evaluated on a uniform grid. The transforms are then handled by FFTs.

Mixed transforms Recall the spectral representation (8) of 2P functions in terms of discrete Fourier series in (x, y) and a continuous transform in z . Hence, the transforms $\mathbf{f}_\eta \rightarrow \widehat{\mathbf{f}}_\eta$ and $\widehat{\psi} \rightarrow \psi$ are mixed. This, together with the exclusion of $\mathbf{k} = 0$ in (45) and the inclusion of the singularity contribution (35), is where our proposed 2P method deviates from the well-established 3P methods.

Fourier integral quadrature Computing the mixed transforms requires two standard discrete Fourier transforms and an approximation of the Fourier integral (in the z -direction). The quadrature step has to be done in the same time-complexity as the discrete transforms; otherwise, the method would not be more efficient than directly summing (21). This is discussed at length in [43], and it is shown to be quite satisfactory to use an FFT-based method (following Press et al. [54, Sec.13.9]) on a moderately oversampled grid.

Spectral accuracy Trapezoidal quadrature applied to (42) is spectrally accurate, due to the C^∞ -regularity of the integrand. Detailed analysis on this appears in [44]. Moreover, the accuracy in computing the Fourier integral in the mixed transform using a simple FFT-based approach strongly depends on the regularity of the integrand.

Grid size corresponds to direct sum truncation As is also extensively discussed in [44], the proposed method enjoys a close relationship between the Ewald sum (21) and the fast method of this section. A finite truncation $|\mathbf{k}| \leq 2\pi k_\infty/L$ of the Ewald sum (21) corresponds to a grid of size $M = 2k_\infty + 1$. Due to the construction of the PME-method based on Gaussians (with C^∞ -regularity), the truncation error from the Ewald sum carries over to the fast method, meaning that the appropriate grid size can be estimated using truncation error estimates for the Ewald sum. This is, as of yet, conjecture in the Stokes 2P setting, verified numerically (cf. Figure 5, right).

Parameters and truncation The free parameter, η , can be used to control the width, denoted w , of the Gaussian used for the convolutions in (44), (42), and we find it natural to prescribe this width in terms of a number of grid points, $w = LP/(2M) = hP/2$. Gaussians lack compact support, but they are highly localized. It is natural to truncate them, as is done in the non-uniform FFT [21, 13]. We let $P \leq M$ denote the number of grid points within the support of each Gaussian, as seen in Figure 4 (bottom). Moreover, it's important to have control of the shape, parameterized with $m > 0$, of the Gaussians (independently of ξ), see Figure 4 (top). It then follows naturally [44] to let

$$\eta = \left(\frac{2w\xi}{m} \right)^2. \quad (46)$$

Periodicity Above, $\|\cdot\|_*$ denotes that periodicity is implied. To prove that (42) equals (19) one needs this notion to be exact (which rules out the well-known ‘‘closest image convention’’). Formally, as Gaussians lack compact support, it should be understood e.g. that $e^{-\beta\|\mathbf{x}-\mathbf{x}_m\|_*^2} := \sum_{\mathbf{p} \in \mathbb{Z}^2} e^{-\beta\|\mathbf{x}-\mathbf{x}_m+\tau(\mathbf{p})\|^2}$. After truncating the Gaussians, this ceases to be relevant – simply extend the domain to accommodate the support of the truncated Gaussians; evaluate (44) on this domain, taking Euclidean distance between particles and grid points; and then additively wrap the extended domain into the original one.

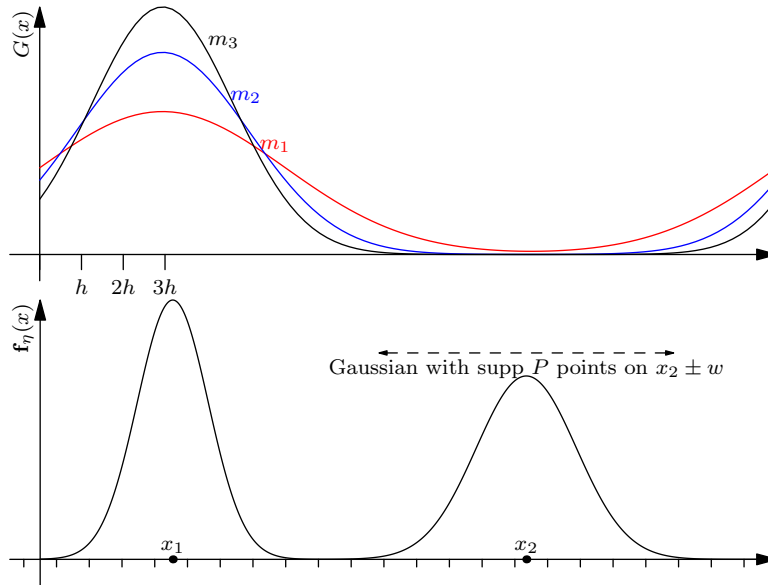


Figure 4: Top: Gaussians with different shape parameters, $m_1 < m_2 < m_3$. Bottom: Gaussian with support on P grid points around \mathbf{x}_j

Approximation errors By approximation errors we mean the errors that the fast SE2P method contributes (in addition to the *spectrum truncation* errors that are inherited from a finite truncation of (21)). These fall into three categories: (i) the numerical error from evaluating the integral (42) with a trapezoidal rule T_P ; (ii) the truncation of the Gaussians; and, finally, (iii) the error in computing the Fourier integral in the mixed transforms. Regarding (i) and (ii), we can prove a detailed error estimate [44, Thm. 3.1], namely that

$$|T_P - \mathbf{u}^F| \leq C \left(e^{-\pi^2 P^2 / (2m^2)} + \operatorname{erfc} \left(m / \sqrt{2} \right) \right). \quad (47)$$

Naturally the first term corresponds to (i) and the second to (ii). It also reveals that if m is taken large the first term goes slower to zero, indicating that selecting $m \approx \sqrt{\pi P}$ strikes a balance between the terms that is favorable for the total error. The final, and $2P$ specific, error concerns the Fourier integral quadrature, and is, as noted above, examined in detail in [43].

Fast gridding The main trade-off for a spectral method is that Gaussians have wider support than e.g. the Cardinal B-splines (used in the SPME method [14]) have. By using the *fast Gaussian gridding* (FGG) procedure, proposed by Greengard & Lee for the non-uniform FFT [21], we mediate this to a large extent. Again, this is examined in [44], and detailed algorithms are given.

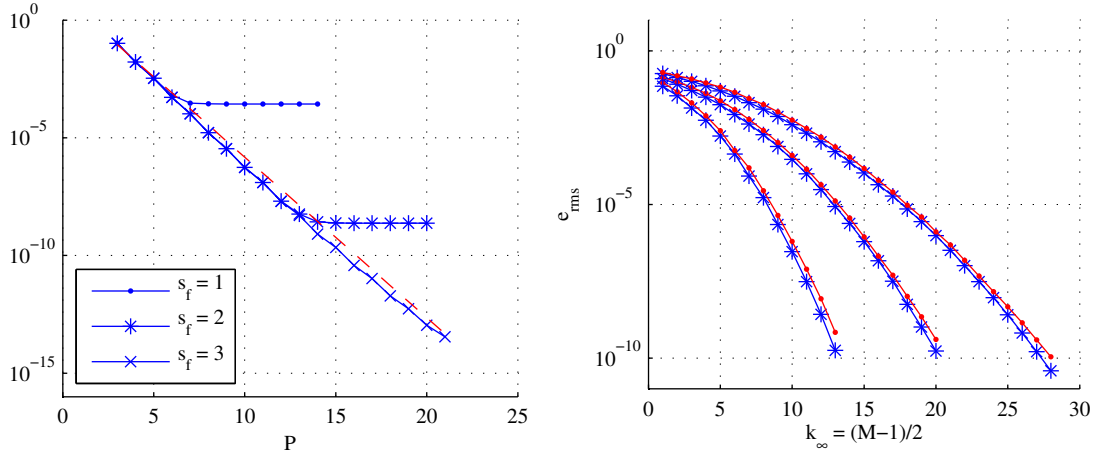


Figure 5: Left: Approximation error in ∞ -norm for SE2P-Stokes method, and (dashed) error estimate (47), as a function of the support of truncated Gaussians, P . Here, $N = 20$, $M = 20$, $\xi = 4$. Right: (*) truncation error for the \mathbf{k} -space Ewald sum (21), vs number of modes κ_∞ (i.e. $|\mathbf{k}| \leq 2\pi\kappa_\infty/L$). As (\cdot) error in SE2P-Stokes method vs. grid size, where P selected to make approximation errors small (left). This isolates the “spectrum truncation” error of the fast method and shows that grid size in the fast method can be selected based error estimates pertaining only to the underlying Ewald sum.

4.3 The singular term

The last term to evaluate is the contribution from the singular integrals that were taken out of the \mathbf{k} -space sum (21),

$$\mathbf{u}^{F,\mathbf{k}=0}(z_m) = -\frac{4}{L^2} \sum_{n=1}^N g(z_m - z_n) \mathbf{I}_2 \mathbf{f}_n.$$

$$g(z) := \pi z \operatorname{erf}(z\xi) + \frac{\sqrt{\pi}}{2\xi} e^{-z^2\xi^2}, \quad (48)$$

cf. the Laplace case [43]. Because g only depends on z it’s almost trivial to compute $\mathbf{u}^{F,\mathbf{k}=0}$ using an interpolation approach. We advocate a Chebyshev method as follows: (i) evaluate $\mathbf{u}^{F,\mathbf{k}=0}(s)$, where s denotes the set of M_0 Gauss-points scaled to the relevant interval; (ii) compute the M_0 coefficients of the interpolating Chebyshev polynomial, $\zeta(z)$, by means of elementary recursions; (iii) evaluate $\mathbf{u}^{F,\mathbf{k}=0}(z_m) \approx \zeta(z_m)$ using a numerically stable Clenshaw formula [54, Sec. 5.4]. Properties of Chebyshev interpolation, including spectral accuracy, are discussed in e.g. Rivlin [56] and many elementary textbooks.

4.4 Parameters, estimates and modus operandi

A commonly cited drawback for Ewald methods, particularly for fast FFT-based ones, is that there are several parameters to choose appropriate values for. For 3P Laplace, this is extensively discussed by Deserno & Holm in their famous survey [12]. Recent results and extensive discussion is found in [70]. In the 2P Laplace case, the situation is, unsurprisingly, quite misty. Kawata & Nagashima [34] have proposed a method, which shares some foundations

with the present work, where it's suggest that an optimization approach be applied to tune a set of eight parameters. The situation is, hopefully, clarified to a large extent in [43].

We suggest that the parameters fall into three natural categories:

1. The desired accuracy, ε , in the computed \mathbf{u} with respect to a particular norm.
2. The Ewald decomposition parameter, ξ , and the truncation of real- and \mathbf{k} -space Ewald sums, r_c and k_∞ , for particular ε .
3. Parameters relating to the fast method:
 - a) the grid size, M , (in each dimension);
 - b) the support, P , and shape, m , of Gaussians, in the FFT-based method for \mathbf{u}^F , and the oversampling factor s_f in the associated mixed transforms;
 - c) the number of Gauss-points, M_0 , in the interpolation method for $\mathbf{u}^{F,\mathbf{k}=0}$.

Item one, choosing ε , comes first – all other parameters will depend on it. We noted that the cost of the real-space sum can vary by orders of magnitude depending on it's implementation and whether a sparse matrix can be assembled and reused or not. With this in mind, we argue that the next consideration should be to select the real-space truncation r_c such that the real-space is cheap to compute.

Item two is clarified by the truncation error estimates of Section 3.3. We noted that, in terms of ε and r_c we can take

$$\xi = \frac{1}{r_c} \sqrt{\log \left(\frac{2}{\varepsilon} \sqrt{\frac{Q r_c}{L^3}} \right)}. \quad (49)$$

That is, ξ is chosen large enough that the error committed by truncating the real-space sum at r_c is close to ε . Fourth, we invoke the equivalence between \mathbf{k} -space truncation and grid in the PME-type method. That is, the truncation error estimate (40) is inverted,

$$k_\infty = \frac{\sqrt{3}L\xi}{2\pi} \sqrt{W \left(\frac{4L^{2/3}\xi^2 Q^{2/3}}{3\pi^{10/3}\varepsilon^{4/3}} \right)}, \quad (50)$$

where $W(\cdot)$ is Lambert W function [10], and the grid size selected as $M = 2k_\infty + 1$.

The remaining parameters, $\{P, m, s_f\}$, are all accuracy parameters, pertaining to the approximation errors added by the fast method, that don't depend on the system. The one with greatest impact on the computational cost is P , the discrete support of the truncated Gaussians, and (cf. Figure 5, left) rough estimates are that $P = 15$ is appropriate for accuracy around 10^{-10} and $P = 23$ is required for full (double-precision) accuracy. As previously determined, it's natural to let $m = C\sqrt{\pi P}$, and we've found that this constant is best taken slightly below unity, $C = 0.92$. The FFT-oversampling in the z -direction, s_f , should be at least two, but should be four or six for higher accuracies (cf. Figure 5). Finally, the number of Gauss-points in the 1D interpolation used to compute $\mathbf{u}^{F,\mathbf{k}=0}$ should be small, $M_0 < 100$, typically around 50.

We would like to emphasize that, although there are a number of parameters to select, the procedure is eminently straight-forward. In particular, PME-grid size selection based on a truncation error estimate for the underlying Ewald sum, is an important feature.

5 Numerical results

In the introduction several areas of ongoing research involving boundary integral methods for Stokes were noted, and we would like to put the present method into that context. This also gives the opportunity to illustrate parameter selection and the practical characteristics of our method.

5.1 Fast boundary integral methods in a periodic setting

As an example, consider a large number of rigid spheres, $\Gamma_i, i = 1 \dots N_s$, in 2P Stokes flow. Let $\tilde{\mathbf{f}}_i$ denote the (unknown) Stokeslet density on Γ_i . Under the constraint of planar periodicity we write the velocity field generated by all $\{\tilde{\mathbf{f}}_i, \Gamma_i\}$ as

$$\mathbf{u}(\mathbf{x}) = \frac{1}{8\pi\mu} \sum_{\mathbf{p} \in \mathbb{Z}^2} \sum_{i=1}^{N_s} \int_{\Gamma_i} S(\mathbf{x} - \mathbf{y} + \tau(\mathbf{p})) \tilde{\mathbf{f}}_i(\mathbf{y}) d\Gamma(\mathbf{y}). \quad (51)$$

Recall that the periodized Stokeslet sum (4) was given a well-defined meaning by the 2P Stokeslet Ewald decomposition (Section 3). The same logic shall apply to (51). We refer the reader to e.g. [51, 71] regarding which Green's functions are required to represent particular flow cases, noting that for this external flow it suffices to use the Stokeslet.

The boundary integral setting is vastly expanded in comparison to the exposition hitherto. Issues that arise, as concisely reviewed in Ying et al. [71], include fast summation methods (to which this work pertains), accurate quadrature rules (surveyed below) and domain boundary representation.

Let each sphere Γ^i be discretized with a set of quadrature points, $\mathbf{x}_j^i, j = 1, \dots, N_p$, and let $T_{\mathbf{x}}$ denote integration with respect to \mathbf{x} by a simple quadrature rule, $T[\zeta] := \sum_j \zeta(\mathbf{x}_j) w_j \approx \int_{\Gamma} \zeta(\mathbf{x}) d\Gamma(\mathbf{x})$. Moreover, let $T^{0,k}$ denote the so-called ‘‘punctured’’ rule, where $w_k \equiv 0$.

For \mathbf{x} on some Γ_i , the integral over Γ_i in (51) is singular when $\mathbf{p} = 0$. Discretizing it in the Nyström fashion, we apply the punctured rule,

$$\begin{aligned} \mathbf{u}^i(\mathbf{x}_m) &\sim \int_{\Gamma_i} S(\mathbf{x}_m - \mathbf{y}) \tilde{\mathbf{f}}(\mathbf{y}) d\Gamma(\mathbf{y}) \\ &\approx T_{\mathbf{y}}^{0,m}[S(\mathbf{x}_m - \mathbf{y}) \tilde{\mathbf{f}}(\mathbf{y})]. \end{aligned}$$

This has one major benefit and one drawback. The benefit is that it renders the discretization of (51) equivalent to the 2P Stokeslet ewald sum (36) – c.f. the exclusion of the term $\{n = m, \mathbf{p} = 0\}$ in the real space sum (17). The drawback is that the punctured rule is only first order accurate.

To obtain higher accuracy, without sacrificing the structure that lets us apply the Ewald decomposition, one can add a local correction, Υ_{loc}^m , to the punctured rule,

$$\mathbf{u}^i(\mathbf{x}_m) \approx T_{\mathbf{y}}^{0,m}[S(\mathbf{x}_m - \mathbf{y}) \tilde{\mathbf{f}}(\mathbf{y})] + \Upsilon_{\text{loc}}^m.$$

Such local corrections to simple quadrature rules (that allow integrable singularities to be handled) have been extensively investigated, and are, of course, unrelated to the planar periodicity of the present problem. Progress has been on a case-by-case basis, with different corrections developed depending on the singularity and the geometry of the boundary, Γ . Early references here include Lyness [47] and Kapur & Rokhlin [33], with subsequent work

by e.g. Aguilar & Chen [1] and Marin et al. [49]. The latter gives formal proofs to the effect, roughly, that on a uniform grid in d dimensions where the singularity has order q and p is the radius (in terms of grid points) of the modified quadrature rule, accuracy of order $\mathcal{O}(h^{2p+2+q+d})$ is attained. Furthermore, Marin et al. in [48] developed such formulas for the Stokeslet, S , though only of the case of Γ being flat.

An alternative that could be expected to yield local corrections, in a way suitable for pairing with fast Ewald methods, is the contour integral formulation of Bazhlekov, Anderson and Meijer [4]. Other alternatives for quadrature over integrable singularities includes *singularity subtraction*, as discussed in the rich survey by Pozrikidis [53], and methods based on carefully selected variable transformations, as discussed in e.g. Sidi [62, 63] and Ying et al. [71].

Moving on, for \mathbf{x}_m on Γ_i , we discretize (51) as

$$\begin{aligned} \mathbf{u}(\mathbf{x}_m) &\approx \frac{1}{8\pi\mu} \left(T_{\mathbf{y}}^{0,m}[S(\mathbf{x}_m - \mathbf{y})\tilde{\mathbf{f}}^i(\mathbf{y})] + \Upsilon_{\text{loc}}^m + \sum_{j=1}^{N_s} \sum_{\mathbf{p} \in \mathbb{Z}^2 \setminus \{0\}} T_{\mathbf{y}}[S(\mathbf{x}_m - \mathbf{y} + \tau(\mathbf{p}))\tilde{\mathbf{f}}^j(\mathbf{y})] \right) \\ &= \frac{1}{8\pi\mu} (\text{Ew}_{2P}(\mathbf{x}, \mathbf{f}) + \Upsilon_{\text{loc}}^m(S, \mathbf{f})). \end{aligned} \quad (52)$$

Here, \mathbf{x} denotes the set of $N = N_s N_p$ discretization points (i.e. $\mathbf{x} = \{\mathbf{x}_j^i : i = 1, \dots, N_s, j = 1, \dots, N_p\}$). Correspondingly, \mathbf{f} denotes the set of discrete Stokeslet strengths multiplied by appropriate quadrature weights, $\mathbf{f} = \{\tilde{\mathbf{f}}_j^i w_j\}$.

The mapping $\mathbf{f} \rightarrow \mathbf{u}$, for fixed \mathbf{x} , is to be understood as a linear system of dimension $3N \times 3N$; knowing \mathbf{u} , we can solve for \mathbf{f} . Such an inversion is by necessity iterative, as the mapping does not have a closed form. Indeed, the Ewald summation method is required to make the action of the periodized Stokeslet convergent (including constraints on \mathbf{f} and physical conditions at $z \rightarrow \pm\infty$).

The fast Ewald method of Section 4 acts as an $\mathcal{O}(N \log N)$ “matvec” operator, for use inside an iterative solver (such as GMRES). The ultimate complexity then depends on the convergence of this iterative procedure (whether the number of GMRES iterations depends on N or not), which leads to the expansive topic of preconditioning; Ying et al. [71] use a method due to Greengard et al. [20], wherein additional references are found.

In this context it’s natural to remark that a second-kind boundary integral formulation is expected to be more advantageous with respect to iteration convergence than the first-kind equation (51). This motivates the development of Ewald decompositions, and associated fast methods, for the double-layer (“doublet” or “stresslet”) Stokes potential.

Finally, it should be noted that investigations of physical systems generally pose the boundary integral problem in a different form. Rather than having boundary conditions for \mathbf{u} on all particles, kinematic conditions (which include boundary integration) are used and the system is closed using force and torque balances. Such a formulation is used for sedimenting fibers [69, 58, 68]. Ewald techniques apply and can handle the main computational task in these sedimentation problems, though additional considerations emerge.

5.2 Stokeslet Ewald as a matvec operator

Having posed a relevant boundary integral problem, we now discuss how to deploy our method in detail and give an indication of how efficient it is. Several of the topics touched upon in the previous section, such as preconditioning and local quadrature correction terms, are beyond

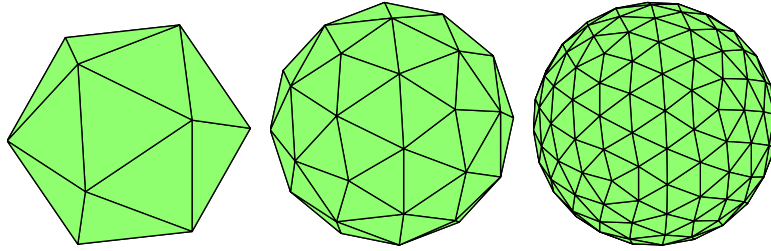


Figure 6: Nearly uniform point distribution on sphere by subdividing icosahedron. Left to right: $N_p = 12, 42, 162$.

the scope of the present work. A central concern is clarifying how to balance the computational cost of the terms in (36).

5.2.1 Parameters, accuracy and cost

We consider a system with N_s spheres, each with a radius r_s , in a domain $\Omega = [0, L]^3$, and assume that the spheres' center are separated by at least $3r_s$. A nearly uniform distribution of points on each sphere, as seen in Figure 6, is obtained by subdividing an icosahedron [45].

We target an accuracy $\varepsilon \approx 10^{-9}$ in the Ewald method. The cost of computing the 2P Stokeslet Ewald sums (17) and (21) depends on the density of the system. Throughout, we shall take an initial number of spheres N_s^0 in a domain with $L = L^0$ and then grow the system at constant density to, say, $L = 3L^0$.

Assuming uniformity, the number of points within a ball with radius r_c is $N_n(r_c) = 4\pi r_c^3 N_s N_p / (3L^3)$. This represents the number of near neighbors that have to be considered for a particular real-space truncation radius, r_c . The cost of computing the real-space sum (cf. Section 4.1) is roughly $N_s N_p N_n(r_c) \lambda$, where λ represents the arithmetic cost associated with each interaction, plus the cost of finding the neighbor list. The factor λ is one (i.e. one floating-point multiply-add) if the real-space sum is computed as a sparse matrix-vector multiplication and on the order of 100-1000 otherwise (because of the computations of $\text{erf}(\cdot)$ and $\text{exp}(\cdot)$).

Table 1 attempts to give an overview of the relationship between real-space sum cost, the system size, and what is then implied for the \mathbf{k} -space sum by the inverted error estimates of Section 4.4. As expected, making the systems denser requires ξ to grow for the cost of the real-space sum (in terms of near neighbors) to remain fixed. Correspondingly, the FFT-grid $M = 2k_\infty$ grows to maintain a fixed accuracy. In what remains, we shall take $P = 16$, the FFTs oversampled by a factor four in the z -direction and $M_0 = 80$ Gauss points in interpolation method for (35). With $r_c = 1/2$, $\xi = 9$, $M = 30$, and \mathbf{x} the points from 5 randomly placed spheres, we compute RMS errors: 2.2×10^{-9} and 6.2×10^{-9} for the real-space sum and SE2P method respectively.

5.2.2 Fast implementations and run-time profiles

In Figures 7 and 8 we give timing results as the system is scaled up and show how the run-time is distributed between the steps in the algorithm. Here we fix the average number of near neighbors at roughly 400 and 1000 respectively, and scale the system up under that constraint. The following remarks clarify the situation:

Given	Derived
$N_s = 100, N_p = 12, N_n = 100$	$r_c = 0.27, \xi = 17.7, k_\infty = 27$
$N_s = 100, N_p = 12, N_n = 1000$	$r_c = 0.58, \xi = 8.3, k_\infty = 12$
$N_s = 100, N_p = 42, N_n = 100$	$r_c = 0.18, \xi = 26.8, k_\infty = 41$
$N_s = 100, N_p = 42, N_n = 1000$	$r_c = 0.38, \xi = 12.5, k_\infty = 19$
$N_s = 1000, N_p = 12, N_n = 100$	$r_c = 0.13, \xi = 37.9, k_\infty = 58$
$N_s = 1000, N_p = 12, N_n = 1000$	$r_c = 0.27, \xi = 17.7, k_\infty = 27$
$N_s = 1000, N_p = 42, N_n = 100$	$r_c = 0.08, \xi = 57.2, k_\infty = 89$
$N_s = 1000, N_p = 42, N_n = 1000$	$r_c = 0.18, \xi = 26.8, k_\infty = 41$

Table 1: Parameter examples for 2P Stokeslet Ewald summation, with $\varepsilon = 10^{-10}$ and $L = 1$. N_s : number of spheres. N_p : number of points per sphere. N_n : number of near neighbors to account for in real-space sum. Right column: parameter values selected based on truncation error estimates (39) and (40).

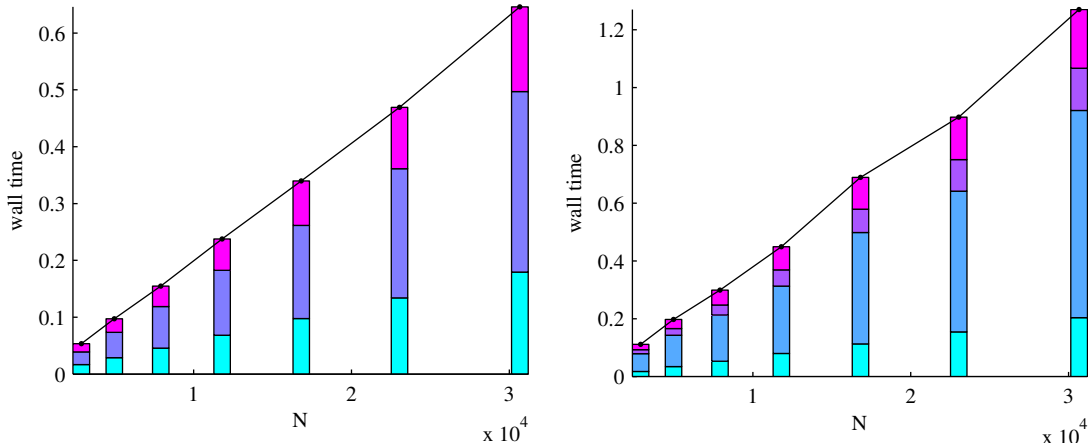
Remark 1 (Real space computation) *The real space sum is evaluated in the matrix form as discussed in Section 4.1. The matrix is computed once and the time to do so is amortized over a hypothetical number of iterations: 50 (which is reasonable, see [58]). This pre-computation contains two parts: first the matrix elements are computed (a), then the sparse matrix is finalized (b). The real-space contribution (17) is computed as a matrix-vector product (c). The bars in Figures 7 and 8 (left) are stacked from bottom to top in the order (a), (b), (c) – showing that, at 50 iterations, constructing the sparse matrix is still the dominating cost.*

Remark 2 (Computation of k-space method) *The tasks in the FFT-based method to compute \mathbf{u}^F are as follows: (a) compute grid function (44); (b) compute oversampled transforms; (c) solve Poisson problem (45); and (d) compute convolution with Gaussians (42). The bar stacks in Figures 7 and 8 (right) breaks down the total time for the method in these steps from bottom to top.*

Our implementation was mostly in Matlab code, and, hence, FFTs were handled by the highly optimized library FFTW [16]³. The code for gridding (44) and integration (42) with the FGG algorithm [21, 44] was implemented in C and the time-critical parts were hand-coded at machine level with SSE instructions and software prefetching. These implementations run close to peak flops of present hardware. An untuned implementation in C runs roughly at a third of the speed, making the gridding steps dominate transforms.

Remark 3 (Computation of $\mathbf{u}^{F, \mathbf{k}=0}$) *The computation of $\mathbf{u}^{F, \mathbf{k}=0}$ as discussed in Section 4.3 involves computing $\pi z \operatorname{erf}(z\xi) + \frac{\sqrt{\pi}}{2\xi} e^{-z^2\xi^2}$ for $z = z_m - z_n$, where $n = 1, \dots, N$ and $m = 1, \dots, M_0$ (the number of Gauss-points for the Chebyshev interpolation). In the iterative*

³By convention, the fast Fourier transform is said to have complexity $\mathcal{O}(N \log N)$, but this concept encompasses a lot of variability which is seen in practice. For instance, an FFT of length 2^n will typically be several times faster than a transform of length $2^n + 1$. The grid sizes seen in the scaling tests here try to avoid the best and worst case transform lengths, to faithfully represent the method.



$\xi = 9, r_c = 1/2, \varepsilon = 10^{-9}, N_n \approx 400$

$L =$	1	1.2	1.4	1.6	1.8	2	2.2
$N_s =$	80	138	220	328	467	640	852
$N =$	2880	4968	7920	11808	16812	23040	30672
$M =$	30	36	42	48	54	60	66

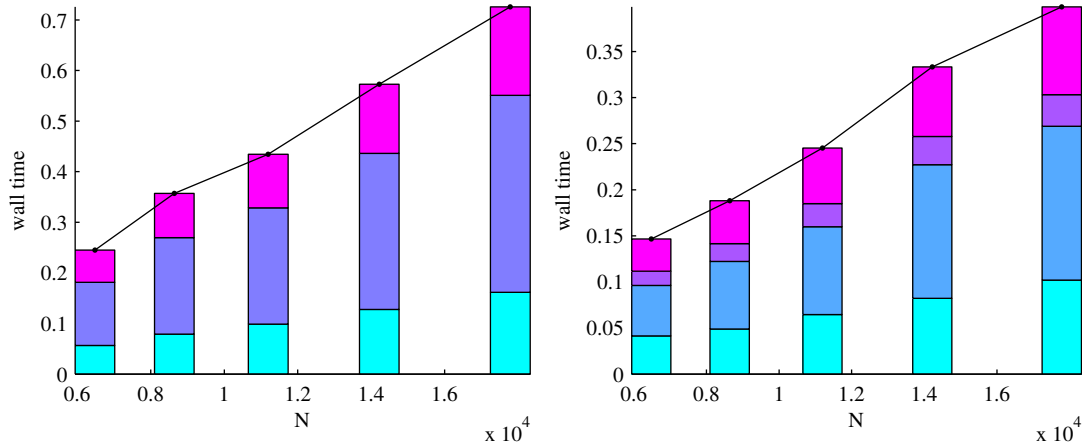
Figure 7: Runtime to compute (36) as system is scaled up, keeping the number of near neighbors fixed at around 400, according to the table above. **Left:** Real-space sum, cf. Remark 1. **Right:** FFT-based \mathbf{k} -space method, cf. Remark 2.

setting, where we wish to rapidly evaluate $\mathbf{u}^{F, \mathbf{k}=0}$ for many \mathbf{f} , this arithmetic should be pre-computed and stored in a matrix, A_0 . Then the sum in (48) is computed by multiplying A_0 with $\mathbf{f}_i, i = 1, 2$. The interpolation procedure follows, which is very fast. Corresponding to the runs in Figures 7 and 8, the times to compute $\mathbf{u}^{F, \mathbf{k}=0}$ were vanishingly small.

We note that balancing the computational cost of the real-space sum and \mathbf{k} -space fast method is non-trivial. At a basic level, it hinges on how dense the system is. Evaluating the real-space sum using a neighbor list method (matrix-form or not) requires the list to be stored. In the iterative setting, the matrix form offers superior performance – so much so that the main constraint of the real-space method becomes memory (i.e. limiting r_c for a particular N). In the fast \mathbf{k} -space method the split in computational burden between transforms and gridding also depends on density – or rather, it depends on the Ewald parameter ξ , which has to increase to keep the number of near neighbors to account for in the real-space sum fixed if the system is made denser.

6 Conclusions

In this paper we have derived a Ewald decomposition for the Stokeslet in planar periodicity (Section 3.2) and a PME-type $\mathcal{O}(N \log N)$ method for the fast evaluation of the resulting expression. The decomposition is the natural 2P counterpart to the classical 3P decomposition by Hasimoto [24]. Truncation error estimates are provided to aid in selecting parameters (Section 3.3). The fast, PME-type, method (Section 4) for computing the \mathbf{k} -space sum (21) is based on a mixed sum/integral form (19), and is similar to the method by the present



$$\xi = 9, r_c = 1/2, \varepsilon = 10^{-9}, N_n \approx 1000$$

$L =$	1	1.1	1.2	1.3	1.4
$N_s =$	180	240	311	395	494
$N =$	6480	8640	11196	14220	17784
$M =$	30	33	36	39	42

Figure 8: Runtime to compute (36) as system is scaled up, keeping the number of near neighbors fixed at around 1000, according to the table above. **Left:** Real-space sum, cf. Remark 1. **Right:** FFT-based \mathbf{k} -space method, cf. Remark 2.

authors [43] for the corresponding problem in electrostatics. This appear to be the first fast method for computing Stokeslet Ewald sums in planar periodicity, and has three attractive properties: it is spectrally accurate; it uses the minimal amount of memory that a gridded Ewald method can use; and a clear view of numerical errors and how to choose parameters is provided (Section 4.4). The final part explores the practicalities of the proposed method, and surveys the computational issues involved in applying it to 2-periodic boundary integral Stokes problems. We presently pursue applications-oriented questions in this regard, and hope to communicate further results in the near future.

A 2P Stokeslet sums, details

A.1 Explicit \mathbf{k} -space form of Stokeslet sum

Here we compute

$$\tilde{\mathbf{u}}(\mathbf{x}_m) = \frac{4}{L^2} \sum_{\mathbf{k} \neq 0} \int_{\mathbb{R}} \left(\frac{\mathbf{I}}{\|\mathbf{k}\|^2} - \frac{\mathbf{k} \otimes \mathbf{k}}{\|\mathbf{k}\|^4} \right) \sum_{n=1}^N \mathbf{f}_n e^{i\mathbf{k} \cdot (\mathbf{x}_m - \mathbf{x}_n)} d\kappa, \quad (53)$$

where $\mathbf{k} = (\mathbf{k}, \kappa) = (k_1, k_2, \kappa)$ is the composition of the discrete and continuous transform variables. The integrals in (53) are computable. We let

$$\tilde{\mathbf{u}}(\mathbf{x}_m) = \frac{4}{L^2} \sum_{\mathbf{k} \neq 0} \sum_{n=1}^N \tilde{Q}(\mathbf{k}, z_m - z_n) \mathbf{f}_n e^{i\mathbf{k} \cdot (\rho_m - \rho_n)},$$

with

$$\begin{aligned}\tilde{Q}(\mathbf{k}, z) &:= \int_{\mathbb{R}} \left(\frac{\mathbf{I}}{\|\mathbf{k}\|^2} - \frac{\mathbf{k} \otimes \mathbf{k}}{\|\mathbf{k}\|^4} \right) e^{i\kappa z} d\kappa \\ &= \int_{\mathbb{R}} \left(\frac{\mathbf{I}}{\|\mathbf{k}\|^2 + \kappa^2} - \frac{\mathbf{k} \otimes \mathbf{k}}{(\|\mathbf{k}\|^2 + \kappa^2)^2} \right) e^{i\kappa z} d\kappa \\ &=: \tilde{Q}_1 + \tilde{Q}_2,\end{aligned}$$

where \tilde{Q}_1 and \tilde{Q}_2 denote integrals over the diagonal- and outer product terms respectively. Note that, since $\mathbf{k} \neq 0$, $k^2 > 0$ and the integrals are nonsingular. We shall encounter integrals of the form

$$L_q^p(k, z) := \int_0^\infty \frac{\kappa^p \cos(\kappa z)}{(k^2 + \kappa^2)^q} d\kappa \quad \text{and} \quad M_q^p(k, z) := \int_0^\infty \frac{\kappa^p \sin(\kappa z)}{(k^2 + \kappa^2)^q} d\kappa,$$

for which we have, with $X = L, M$, that

$$X_{q+1}^p = -\frac{1}{2kq} \frac{\partial X_q^p}{\partial k}, \quad q \in \mathbb{Z}, q > 0. \quad (54)$$

Evidently,

$$\tilde{Q}_1(\mathbf{k}, z) = 2\mathbf{I}L_1^0(\|\mathbf{k}\|, z). \quad (55)$$

The integral here is known [74, 3.723(2), p. 424],

$$L_1^0(k, z) = \frac{\pi e^{-k|z|}}{2k}, \quad k > 0.$$

To simplify matters in computing \tilde{Q}_2 – reducing the number of integrals to labor over – we note that the integrand can be viewed as an *element-wise* multiplication of

$$(\mathbf{k}, 1) \otimes (\mathbf{k}, 1) = \begin{bmatrix} k_1^2 & k_1 k_2 & k_1 \\ k_1 k_2 & k_2^2 & k_2 \\ k_1 & k_2 & 1 \end{bmatrix}$$

and

$$\frac{(1, 1, \kappa) \otimes (1, 1, \kappa)}{(\|\mathbf{k}\|^2 + \kappa^2)^2} = (\|\mathbf{k}\|^2 + \kappa^2)^{-2} \begin{bmatrix} 1 & 1 & \kappa \\ 1 & 1 & \kappa \\ \kappa & \kappa & \kappa^2 \end{bmatrix}$$

where the former is a constant under the integration. The latter demonstrates that there are three integrals to compute and arrange as:

$$\tilde{Q}_2(\mathbf{k}, z) = -2 \begin{bmatrix} k_1^2 L_2^0(\|\mathbf{k}\|, z) & k_1 k_2 L_2^0(\|\mathbf{k}\|, z) & i k_1 M_2^1(\|\mathbf{k}\|, z) \\ k_1 k_2 L_2^0(\|\mathbf{k}\|, z) & k_2^2 L_2^0(\|\mathbf{k}\|, z) & i k_2 M_2^1(\|\mathbf{k}\|, z) \\ i k_1 M_2^1(\|\mathbf{k}\|, z) & i k_2 M_2^1(\|\mathbf{k}\|, z) & L_2^2(\|\mathbf{k}\|, z) \end{bmatrix}.$$

Having already found L_1^0 , (54) gives that

$$L_2^0(k, z) = \frac{\pi e^{-k|z|}(k|z| + 1)}{4k^3}.$$

Moreover, $L_2^2 = L_0^0 - k^2 L_2^0$, so that

$$L_2^2(k, z) = -\frac{\pi e^{-k|z|}(k|z| - 1)}{4k},$$

by (54). Finally,

$$M_2^1(k, z) = -\frac{\partial}{\partial z} L_2^0(k, z) = \frac{\pi z e^{-k|z|}}{4k}.$$

Thus, we have obtained an explicit form of the \mathbf{k} -space 2P Stokeslet sum (53):

$$\tilde{\mathbf{u}}(\mathbf{x}_m) = \frac{4}{L^2} \sum_{\mathbf{k} \neq 0} \sum_{n=1}^N \tilde{Q}(\mathbf{k}, z_m - z_n) \mathbf{f}_n e^{i\mathbf{k} \cdot (\rho_m - \rho_n)},$$

where

$$\begin{aligned} \tilde{Q}(\mathbf{k}, z) &= 2 \begin{bmatrix} L_1^0 - k_1^2 L_2^0 & -k_1 k_2 L_2^0 & -i k_1 M_2^1 \\ -k_1 k_2 L_2^0 & L_1^0 - k_2^2 L_2^0 & -i k_2 M_2^1 \\ -i k_1 M_2^1 & -i k_2 M_2^1 & L_1^0 - L_2^2 \end{bmatrix} (\|\mathbf{k}\|, z) \\ &= \frac{e^{-\|\mathbf{k}\||z|}}{\|\mathbf{k}\|} \begin{bmatrix} \pi - \frac{(\pi\|\mathbf{k}\||z| + \pi)k_1^2}{2\|\mathbf{k}\|^2} & -\frac{\pi(\|\mathbf{k}\||z| + 1)k_1 k_2}{2\|\mathbf{k}\|^2} & -\frac{1}{2}i\pi z k_1 \\ -\frac{\pi(\|\mathbf{k}\||z| + 1)k_1 k_2}{2\|\mathbf{k}\|^2} & \pi - \frac{(\pi\|\mathbf{k}\||z| + \pi)k_2^2}{2\|\mathbf{k}\|^2} & -\frac{1}{2}i\pi z k_2 \\ -\frac{1}{2}i\pi z k_1 & -\frac{1}{2}i\pi z k_2 & \frac{1}{2}(\pi\|\mathbf{k}\||z| + \pi) \end{bmatrix}. \end{aligned}$$

A.2 Explicit \mathbf{k} -space form of regularized Stokeslet sum

Our objective here is to compute the integral Q , given in (20), to obtain an explicit 2P Stokeslet Ewald sum. The tensor B (7) contains a diagonal and an outer product term, and we integrate them separately. That is, let

$$Q(\mathbf{k}, z) = Q^{\mathbf{I}}(\mathbf{k}, z) + Q^{\mathbf{k} \otimes \mathbf{k}}(\mathbf{k}, z),$$

where

$$\begin{aligned} Q^{\mathbf{I}}(\mathbf{k}, z) &= \mathbf{I} e^{-\|\mathbf{k}\|^2/4\xi^2} \int_{\mathbb{R}} \left(\frac{1}{4\xi^2} + \frac{1}{\|\mathbf{k}\|^2} \right) e^{-\kappa^2/4\xi^2} e^{i\kappa z} d\kappa \\ &= \mathbf{I} e^{-\|\mathbf{k}\|^2/4\xi^2} \int_{\mathbb{R}} \left(\frac{1}{4\xi^2} + \frac{1}{\|\mathbf{k}\|^2 + \kappa^2} \right) e^{-\kappa^2/4\xi^2} e^{i\kappa z} d\kappa \end{aligned}$$

and

$$\begin{aligned} Q^{\mathbf{k} \otimes \mathbf{k}}(\mathbf{k}, z) &= -e^{-\|\mathbf{k}\|^2/4\xi^2} \int_{\mathbb{R}} \left(\frac{1}{4\xi^2\|\mathbf{k}\|^2} + \frac{1}{\|\mathbf{k}\|^4} \right) (\mathbf{k} \otimes \mathbf{k}) e^{-\kappa^2/4\xi^2} e^{i\kappa z} d\kappa \\ &= -e^{-\|\mathbf{k}\|^2/4\xi^2} \int_{\mathbb{R}} \left(\frac{1}{4\xi^2(\|\mathbf{k}\|^2 + \kappa^2)} + \frac{1}{(\|\mathbf{k}\|^2 + \kappa^2)^2} \right) (\mathbf{k} \otimes \mathbf{k}) e^{-\kappa^2/4\xi^2} e^{i\kappa z} d\kappa. \end{aligned}$$

For non-negative integers p and q we let

$$\tilde{J}_q^p(k, z) := \int_0^\infty \frac{\kappa^p \cos(\kappa z)}{(k^2 + \kappa^2)^q} e^{-\kappa^2/4\xi^2} d\kappa, \quad J_q^p(k, z) := e^{-k^2/4\xi^2} \tilde{J}_q^p(k, z)$$

and

$$\tilde{K}_q^p(k, z) := \int_0^\infty \frac{\kappa^p \sin(\kappa z)}{(k^2 + \kappa^2)^q} e^{-\kappa^2/4\xi^2} d\kappa, \quad K_q^p(k, z) := e^{-k^2/4\xi^2} \tilde{K}_q^p(k, z).$$

With these definitions, it is evident that

$$Q^{\mathbf{I}}(\mathbf{k}, z) = 2 \left(\frac{J_0^0(z)}{4\xi^2} + J_0^1(\|\mathbf{k}\|, z) \right) \mathbf{I}.$$

The first integral is elementary,

$$\tilde{J}_0^0(z) = \sqrt{\pi}\xi e^{-z^2\xi^2}, \quad (56)$$

and the second can be found [74, 3.954(2), p. 504]

$$\tilde{J}_1^0(k, z) = \frac{\pi e^{k^2/4\xi^2}}{4k} \left(e^{-kz} \operatorname{erfc} \left(\frac{k}{2\xi} - z\xi \right) + e^{kz} \operatorname{erfc} \left(\frac{k}{2\xi} + z\xi \right) \right), \quad k > 0. \quad (57)$$

Moving on to $Q^{\mathbf{k} \otimes \mathbf{k}}$, one studies the symmetries of the integrand as when computing \tilde{Q}_2 , to find that

$$Q^{\mathbf{k} \otimes \mathbf{k}}(\mathbf{k}, z) = -2 \begin{bmatrix} k_1^2 \left(\frac{J_1^0}{4\xi^2} + J_2^0 \right) & k_1 k_2 \left(\frac{J_1^0}{4\xi^2} + J_2^0 \right) & k_1 \left(\frac{iK_1^1}{4\xi^2} + iK_2^1 \right) \\ k_1 k_2 \left(\frac{J_1^0}{4\xi^2} + J_2^0 \right) & k_2^2 \left(\frac{J_1^0}{4\xi^2} + J_2^0 \right) & k_2 \left(\frac{iK_1^1}{4\xi^2} + iK_2^1 \right) \\ k_1 \left(\frac{iK_1^1}{4\xi^2} + iK_2^1 \right) & k_2 \left(\frac{iK_1^1}{4\xi^2} + iK_2^1 \right) & \frac{J_1^2}{4\xi^2} + J_2^2 \end{bmatrix} (\|\mathbf{k}\|, z).$$

The integrals present are related, as previously, via (54) and obvious algebraic relationships. With \tilde{J}_0^0 and \tilde{J}_1^0 known, one finds

$$\begin{aligned} \tilde{J}_2^0(k, z) &= -\frac{1}{2k} \frac{\partial}{\partial k} \tilde{J}_1^0(k, z) \\ \tilde{J}_1^2(k, z) &= \tilde{J}_0^0(k, z) - k^2 \tilde{J}_2^0(k, z) \\ \tilde{J}_2^2(k, z) &= -\frac{1}{2k} \frac{\partial}{\partial k} \tilde{J}_1^2(k, z). \end{aligned}$$

Moving on to the anti-symmetric integrals K_q^p , one can find [74, 3.954(1), p. 504]

$$\tilde{K}_1^1(k, z) = \frac{\pi e^{k^2/4\xi^2}}{4} \left(e^{-kz} \operatorname{erfc} \left(\frac{k}{2\xi} - z\xi \right) - e^{kz} \operatorname{erfc} \left(\frac{k}{2\xi} + z\xi \right) \right),$$

and, consequently,

$$\tilde{K}_2^1(k, z) = -\frac{1}{2k} \frac{\partial}{\partial k} \tilde{K}_1^1(k, z).$$

This completes the delicate matter of integration. There remains to find compact expressions for the J_q^p - and K_q^p terms that were left as derivatives above. The forms of (56) and (57) suggest that we look for terms

$$\begin{aligned} \lambda &:= e^{-k^2/4\xi^2 - \xi^2 z^2} \\ \theta_+ &:= e^{kz} \operatorname{erfc} \left(\frac{k}{2\xi} + \xi z \right) \\ \theta_- &:= e^{-kz} \operatorname{erfc} \left(\frac{k}{2\xi} - \xi z \right). \end{aligned}$$

With this, explicit forms of J_q^p and K_q^p , as given in (27)-(33) follow.

B Conventions for Fourier transforms and series

For compactness, we use a non-unitary form of the Fourier transform. For a function, $f(\mathbf{x})$, $\mathbf{x} \in \mathbb{R}^n$, which is periodic with respect to $\Omega \subset \mathbb{R}^n$, we have the Fourier series defined as

$$f(\mathbf{x}) = \sum_{\mathbf{k}} \hat{f}_{\mathbf{k}} e^{i\mathbf{k}\cdot\mathbf{x}}$$
$$\hat{f}_{\mathbf{k}} = \frac{1}{|\Omega|} \int_{\Omega} f(\mathbf{x}) e^{-i\mathbf{k}\cdot\mathbf{x}} d\mathbf{x},$$

where $\mathbf{k} \in \{2\pi\mathbf{n}/L : \mathbf{n} \in \mathbb{Z}^n\}$. The corresponding integral transform for functions that decay sufficiently fast on \mathbb{R}^n is then naturally

$$f(\mathbf{x}) = \frac{1}{(2\pi)^n} \int_{\mathbb{R}^n} \hat{f}(\bar{\mathbf{k}}) e^{i\bar{\mathbf{k}}\cdot\mathbf{x}} d\bar{\mathbf{k}}$$
$$\hat{f}(\bar{\mathbf{k}}) = \int_{\mathbb{R}^n} f(\mathbf{x}) e^{-i\bar{\mathbf{k}}\cdot\mathbf{x}} d\mathbf{x}, \quad \bar{\mathbf{k}} \in \mathbb{R}^n.$$

References

- [1] J. C. Aguilar and Y. Chen. High-order corrected trapezoidal quadrature rules for the Coulomb potential in three dimensions. *Comput. Math. Appl.*, 49:625–631, February 2005.
- [2] A. Arnold, J. de Joannis, and C. Holm. Electrostatics in periodic slab geometries. I. *J. Chem. Phys.*, 117:2496–2502, 2002.
- [3] G. K. Batchelor. Slender-body theory for particles of arbitrary cross-section in Stokes flow. *J. Fluid Mech.*, 44:419–440, 1970.
- [4] I. Bazhlekov, P. Anderson, and H. Meijer. Nonsingular boundary integral method for deformable drops in viscous flows. *Phys. Fluids*, 16:1064–1081, April 2004.
- [5] I. Bazhlekov, P. Anderson, and H. Meijer. Numerical investigation of the effect of insoluble surfactants on drop deformation and breakup in simple shear flows. *J. Colloid. Interf. Sci.*, 298:369–394, 2006.
- [6] J. F. Brady and G. Bossis. Stokesian Dynamics. *Annu. Rev. Fluid Mech.*, 20:111–157, 1988.
- [7] J. E. Butler and E. S. G. Shaqfeh. Dynamic simulations of the inhomogeneous sedimentation of rigid fibres. *J. Fluid Mech.*, 468:205–237, October 2002.
- [8] S. Childress, S. E. Spagnolie, and T. Tokieda. A bug on a raft: recoil locomotion in a viscous fluid. *J. Fluid Mech.*, 669:527–556, February 2011.
- [9] N. Coq, A. Bricard, F.-D. Delapierre, L. Malaquin, O. du Roure, M. Fermigier, and D. Bartolo. Collective beating of artificial microcilia. *Phys. Rev. Lett.*, 107:014501, Jun 2011.
- [10] R. M. Corless, G. H. Gonnet, D. E. G. Hare, D. J. Jeffrey, and D. E. Knuth. On the Lambert W function. *Adv. Comput. Math.*, 5:329–359, 1996.

- [11] T. Darden, D. York, and L. Pedersen. Particle mesh Ewald - an $N \cdot \log(N)$ method for Ewald sums in large systems. *J. Chem. Phys.*, 98:10089–10092, 1993.
- [12] M. Deserno and C. Holm. How to mesh up Ewald sums. I. A theoretical and numerical comparison of various particle mesh routines. *J. Chem. Phys.*, 109:7678–7693, 1998.
- [13] A. Dutt and V. Rokhlin. Fast Fourier-transforms for nonequispaced data. *SIAM J. Sci. Comput.*, 14:1368–1393, 1993.
- [14] U. Essmann, L. Perera, M. L. Berkowitz, T. Darden, H. Lee, and L. G. Pedersen. A smooth particle mesh Ewald method. *J. Chem. Phys.*, 103:8577–8593, 1995.
- [15] D. Frenkel and B. Smit. *Understanding Molecular Simulation*. Academic Press, 2 edition, 11 2001.
- [16] M. Frigo and S. G. Johnson. The design and implementation of FFTW3. *P. IEEE*, 93:216–231, 2005.
- [17] D. Gonzalez-Rodriguez and E. Lauga. Reciprocal locomotion of dense swimmers in Stokes flow. *J. Phys.-Condens. Mat.*, 21:204103, May 2009.
- [18] T. Götz. Simulating particles in Stokes flow. *J. Comput. Appl. Math.*, 175:415–427, 2005.
- [19] L. Greengard and M. C. Kropinski. Integral equation methods for Stokes flow in doubly-periodic domains. *J. Eng. Math.*, 48:157–170, 2004.
- [20] L. Greengard, M. C. Kropinski, and A. Mayo. Integral equation methods for Stokes flow and isotropic elasticity in the plane. *J. Comput. Phys.*, 125:403–414, May 1996.
- [21] L. Greengard and JY Lee. Accelerating the nonuniform fast Fourier transform. *SIAM Rev.*, 46(3):443–454, 2004.
- [22] L. Greengard and V. Rokhlin. A fast algorithm for particle simulations. *J. Comput. Phys.*, 73:325–348, 1987.
- [23] A. Grzybowski, E. Gwozdz, and A. Brodka. Ewald summation of electrostatic interactions in molecular dynamics of a three-dimensional system with periodicity in two directions. *Phys. Rev. B*, 61:6706–6712, 2000.
- [24] H. Hasimoto. On the periodic fundamental solutions of the Stokes equations and their application to viscous flow past a cubic array of spheres. *J. Fluid Mech*, 5:317–328, 1959.
- [25] J. P. Hernandez-Ortiz, J. J. de Pablo, and M. D. Graham. Fast computation of many-particle hydrodynamic and electrostatic interactions in a confined geometry. *Phys. Rev. Lett.*, 98, April 2007.
- [26] R.W. Hockney and J.W. Eastwood. *Computer Simulation Using Particles*. McGraw-Hill, New York, 1981.
- [27] I. D. Hosein and C. M. Liddell. Convectively assembled asymmetric dimer-based colloidal crystals. *Langmuir*, 23:10479–10485, October 2007.

- [28] K. Ishii. Viscous-flow past multiple planar arrays of small spheres. *J. Phys. Soc. Jpn.*, 46:675–680, 1979.
- [29] T. Ishikawa, G. Sekiya, Y. Imai, and T. Yamaguchi. Hydrodynamic interactions between two swimming bacteria. *Biophys. J.*, 93:2217–2225, September 2007.
- [30] T. Ishikawa, M. P. Simmonds, and T. J. Pedley. Hydrodynamic interaction of two swimming model micro-organisms. *J. Fluid Mech.*, 568:119–160, December 2006.
- [31] P. J. A. Janssen and P. D. Anderson. Boundary-integral method for drop deformation between parallel plates. *Phys. Fluids*, 19:043602, April 2007.
- [32] A. Kanevsky, M. J. Shelley, and A.-K. Tornberg. Modeling simple locomotors in Stokes flow. *J. Comput. Phys.*, 229:958–977, February 2010.
- [33] S. Kapur and V. Rokhlin. High-order corrected trapezoidal quadrature rules for singular functions. *SIAM J. Numer. Anal.*, 34:1331–1356, August 1997.
- [34] M. Kawata and U. Nagashima. Particle mesh Ewald method for three-dimensional systems with two-dimensional periodicity. *Chem. Phys. Lett.*, 340:165–172, 2001.
- [35] E. E. Keaveny and M. J. Shelley. Applying a second-kind boundary integral equation for surface tractions in Stokes flow. *J. Comput. Phys.*, 230:2141–2159, March 2011.
- [36] S. N. Khaderi, M. G. H. M. Baltussen, P. D. Anderson, D. Ioan, J. M. J. den Toonder, and P. R. Onck. Nature-inspired microfluidic propulsion using magnetic actuation. *Phys. Rev. E*, 79:046304, Apr 2009.
- [37] J. Koiller, K. Ehlers, and R. Montgomery. Problems and progress in microswimming. *J. Nonlinear Sci.*, 6:507–541, November 1996.
- [38] G. Kokot, Vilfan M, N. Osterman, A. Vilfan, B. Kavcic, I. Poberaj, and D. Babic. Measurement of fluid flow generated by artificial cilia. *Biomicrofluidics*, 5(3):034103, 2011.
- [39] J. Kolafa and J. W. Perram. Cutoff errors in the Ewald summation formulas for point-charge systems. *Mol. Simulat.*, 9:351–368, 1992.
- [40] K. N. Kudin and G. E. Scuseria. Revisiting infinite lattice sums with the periodic fast multipole method. *J. Chem. Phys.*, 121:2886–2890, 2004.
- [41] A. Kumar and J. J. L. Higdon. Particle mesh Ewald Stokesian dynamics simulations for suspensions of non-spherical particles. *J. Fluid Mech.*, 675:297–335, May 2011.
- [42] D. Lindbo and A.-K. Tornberg. Spectrally accurate fast summation for periodic Stokes potentials. *J. Comput. Phys.*, 229:8994 – 9010, 2010.
- [43] D. Lindbo and A.-K. Tornberg. Fast and spectrally accurate Ewald summation for 2-periodic electrostatic systems. arXiv:1109.1667 (2011), <http://arxiv.org/abs/1109.1667>, 2011.
- [44] D. Lindbo and A.-K. Tornberg. Spectral accuracy in fast Ewald-based methods for particle simulations. *J. Comput. Phys.*, 230:8744–8761, 2011.

- [45] G. Luigi. Matlab code: BuildSphere. <http://giaccariluigi.altervista.org/blog/>, April 2009. Retrieved 08/19/2011.
- [46] F. Lundell, L. D. Söderberg, and P. H. Alfredsson. Fluid mechanics of papermaking. *Annu. Rev. Fluid Mech.*, 43:195–217, 2011.
- [47] J. N. Lyness. Error functional expansion for N-dimensional quadrature with an integrand function singular at a point. *Math. Comput.*, 30:1–23, 1976.
- [48] O. Marin, K. Gustavsson, and A.-K. Tornberg. A wall treatment for confined Stokes flow. In preparation, 2011.
- [49] O. Marin, O. Runborg, and A.-K. Tornberg. Corrected trapezoidal rules for a class of singular functions. In preparation, 2011.
- [50] M. Mazars. Lekner summations and Ewald summations for quasi-two-dimensional systems. *Mol. Phys.*, 103:1241–1260, 2005.
- [51] C. Pozrikidis. *Boundary Integral and Singularity Methods for Linearized Viscous Flow*. Cambridge University Press, 1992.
- [52] C. Pozrikidis. Computation of periodic Green’s functions of Stokes flow. *J. Eng. Math.*, 30:79–96, 1996.
- [53] C. Pozrikidis. Interfacial dynamics for Stokes flow. *J. Comput. Phys.*, 169:250–301, 2001.
- [54] W. H. Press, S. A. Teukolsky, W. T. Vetterling, and B. P. Flannery. *Numerical Recipes 3rd Edition: The Art of Scientific Computing*. Cambridge University Press, 2007.
- [55] E. M. Purcell. Life at low Reynolds-number. *Am. J. Phys.*, 45:3–11, 1977.
- [56] T. J. Rivlin. *Chebyshev Polynomials: From Approximation Theory to Algebra and Number Theory*. Wiley-Interscience, 2 edition, 1990.
- [57] S. K. Saha and G. P. Celata. Advances in modelling of biomimetic fluid flow at different scales. *Nanoscale Res. Lett.*, 6:344, April 2011.
- [58] D. Saintillan, E. Darve, and E. S. G. Shaqfeh. A smooth particle-mesh Ewald algorithm for Stokes suspension simulations: The sedimentation of fibers. *Phys. Fluids*, 17, March 2005.
- [59] D. Saintillan and M. J. Shelley. Orientational order and instabilities in suspensions of self-locomoting rods. *Phys. Rev. Lett.*, 99:058102, August 2007.
- [60] Y. B. Shan, J. L. Klepeis, M. P. Eastwood, R. O. Dror, and D. E. Shaw. Gaussian split Ewald: A fast Ewald mesh method for molecular simulation. *J. Chem. Phys.*, 122:054101, 2005.
- [61] M. J. Shelley and T. Ueda. The Stokesian hydrodynamics of flexing, stretching filaments. *Physica D*, 146:221 – 245, 2000.
- [62] A. Sidi. Numerical integration over smooth surfaces in R-3 via class S(m) variable transformations. Part II: Singular integrands. *Appl. Math. Comput.*, 181:291–309, October 2006.

- [63] A. Sidi. Further extension of a class of periodizing variable transformations for numerical integration. *J. Comput. Appl. Math.*, 221:132–149, November 2008.
- [64] A. Sierou and J. F. Brady. Accelerated Stokesian Dynamics simulations. *J. Fluid Mech.*, 448:115–146, 2001.
- [65] S. E. Spagnolie and E. Lauga. Jet propulsion without inertia. *Phys. Fluids*, 22:081902, August 2010.
- [66] S. E. Spagnolie and E. Lauga. The optimal elastic flagellum. *Phys. Fluids*, 22:031901, March 2010.
- [67] H. Takemoto, T. Ohyama, and A. Tohsaki. Direct sum of Coulomb potential without ambiguities of conditionally convergent series. *Prog. Theor. Phys.*, 109:563–573, 2003.
- [68] A.-K. Tornberg and K. Gustavsson. A numerical method for simulations of rigid fiber suspensions. *J. Comput. Phys.*, 215:172–196, June 2006.
- [69] A.-K. Tornberg and M. J. Shelley. Simulating the dynamics and interactions of flexible fibers in Stokes flows. *J. Comput. Phys.*, 196:8–40, May 2004.
- [70] H. Wang, F. Dommert, and C. Holm. Optimizing working parameters of the smooth particle mesh Ewald algorithm in terms of accuracy and efficiency. *J. Chem. Phys.*, 133:034117, July 2010.
- [71] L. X. Ying, G. Biros, and D. Zorin. A high-order 3d boundary integral equation solver for elliptic pdes in smooth domains. *J. Comput. Phys.*, 219(1):247–275, 2006.
- [72] Y. N. Young, M. R. Booty, M. Siegel, and J. Li. Influence of surfactant solubility on the deformation and breakup of a bubble or capillary jet in a viscous fluid. *Phys. Fluids*, 21, July 2009.
- [73] H. Zhou and C. Pozrikidis. Adaptive singularity method for Stokes flow past particles. *J. Comput. Phys.*, 117:79 – 89, 1995.
- [74] D. Zwillinger, editor. *Table of Integrals, Series, and Products, Seventh Edition*. Academic Press, 2007.